MODELING SPECIAL NUCLEAR MATERIAL DIVERSION FROM A MODULAR PYROPROCESSING FACILITY

BY

GREG T. WESTPHAL

THESIS

Submitted in partial fulfillment of the requirements
for the degree of Master of Science in Nuclear, Plasma, and Radiological Engineering
in the Graduate College of the
University of Illinois at Urbana-Champaign, 2019

Urbana, Illinois

Master's Committee:

Assistant Professor Kathryn Huff, Advisor
Professor James F. Stubbins

Abstract

As a result of the once-through fuel cycle implemented in the US, used nuclear fuel (UNF) steadily increases. One proposed solution is the transition to a closed nuclear fuel cycle, in which reprocessing reduces build up of UNF. Pyroprocessing is an attractive method for this transition for its capabilities separating both LWR and metallic fuels, and inherit proliferation resistance. However, unlike aqueous reprocessing plants, industrial pyroprocessing plants do not yet exist. Similar to safety-by-design in next generation of reactors, safeguards-by-design should be a part of reprocessing. Without operational experience, these safeguards-by-design need to be derived through modeling and simulation.

This thesis develops a medium fidelity generic model, Pyre, capable of simulating a variety of facility configurations. Pyre also allows diversion through a diverter class capable of tracking signatures and observables. Rather than track exact material production we use signatures and observables such as operating temperature, pressure, and current to mimic the capabilities of IAEA inspections.

These capabilities are verified in a transition-scenario of the current US fuel cycle to an SFR-based closed fuel cycle. Key operating parameters are determined through sensitivity analysis on this scenario, monitoring isotopic changes in material unaccounted for.

Acknowledgments

First and foremost I would like to thank my advisor Kathryn Huff for her patient guidance and introduction to software development, as well as her support troubleshooting along the way. For their help starting out with Cyclus, multiple debugging efforts, and much more thank you to Gwendolyn Chee and Teddy Bae. Also my classmates Roberto Fairhurst, Anshuman Chuabe, Sun Myung Park, and Mark Kamuda whose support was a great help. Finally, thank you to my parents and brothers for their never-ending support and feedback. This material is based upon work supported by the Department of Energy National Nuclear Security Administration under Award Number(s) DE-NA0002576 through the Consortium for Nonproliferation Enabling Capabilities.

Table of Contents

Chapter 1

Introduction

The diversion of significant quantities of Special Nuclear Material (SNM) from the nuclear fuel cycle is a major non-proliferation concern [1]. These diversions must be detected in a timely manner using signatures and observables in order to properly safeguard the fuel cycle. Timely detection is critical in non-proliferation to discover these shadow fuel cycles before diverted material is further processed. Pyroprocessing is a used nuclear fuel separations technology for advanced reactors. The goal of this research is to identify potential signs of material diversion in a pyroprocessing facility and implement models of these processes into a detailed pyroprocessing facility archetype to the modular, agent-based fuel cycle simulator, Cyclus [2]. This facility archetype will equip users of the Cyclus fuel cycle simulator to investigate detection timeliness enabled by measuring signatures and observables in various fuel cycle scenarios.

1.1 Motivation

1.1.1 Future Fuel Cycles

As the world begins to consider cleaner forms of energy in response to climate change, nuclear energy has regained traction. A main concern with nuclear power is the pileup of used nuclear fuel (UNF) as a result of the once-through fuel cycle. One suggested solution is converting to a closed fuel cycle [3]. There are many approaches to transitioning from our current fuel cycle to a new or closed cycle. Of these future fuel cycles, those involving

sodium fast reactors (SFRs) are of interest. Pyroprocessing enables a transition from light water reactors (LWRs) to SFRs and other metallic fuel. Therefore, pyroprocessing is under consideration as a means of processing the fuel required to start up new breeder reactors for the EG01-EG24 transition scenario.

1.1.2 Pyroprocessing

For other fuel cycle facilities, we have plenty of operating experience to inform safeguards. For example, in the case of aqueous reprocessing the International Atomic Energy Agency (IAEA) provides detailed flow-sheets of existing facilities [4]. Multiple modeling tools have been developed for electrochemical processes such as the Separation and Safeguards Performance Model (SSPM) and Argonne Model for Pyrochemical Recycling (AMPYRE) to combat this lack of operational experience for pyroprocessing plants [5]. These tools take a high fidelity approach to model the chemistry taking place within each chamber. In order to run these tools, the user must have intimate knowledge of the specific facility the flowsheets have been designed for. There is a gap, however, in the medium fidelity models that can inform broader fuel cycle applications such as transition scenarios [6].

1.1.3 Safeguards

Currently there are no commercially operated pyroprocessing plants, however various research designs exist in national labs, notably Argonne National Lab (ANL), Idaho National Lab (INL), and the Korea Atomic Energy Research Institute (KAERI) [7, 8, 9]. Therefore, prior to construction of any design we want to implement safeguards by design. Similar to security by design in next generation reactors, safeguards-by-design incorporates key measurement points and access points into the facility design. Rather than learn from mistakes, in the future we aim to incorporate safety into the design.

1.2 Background

Prior work has been done on modeling high fidelity facilities and pyroprocessing. In the following section we compile recent efforts modeling fuel cycle facilities with Cyclus. I also breakdown the electrochemical processes of each sub-process in generic pyroprocessing operation. The key elements are voloxidation, electroreduction, electrorefining, and electrowinning.

1.2.1 Facility Modeling

Developers at the University of Wisconsin, University of Tennessee Knoxville, and University of Texas Austin have created a number of detailed facility models to expand the Cyclus framework. At Wisconsin, Dr. Meghan McGarry contributed various random number generator (RNG) based archetypes to capture non-deterministic behaviors in `Enrich` and `Sink` [10]. The capabilities for these archetypes include variable assays, inspector swipe tests, and Gaussian distribution of material. `CascadeEnrich` adds further detail to the `Enrich` archetype by incorporating detailed centrifuge physics and parameters. Current work from Wisconsin includes work from graduate student Kathryn Mummah, who is using pathway analysis to identify key diversion paths within Cyclus simulations [11]. Her work also focuses on the addition of sub-facility modeling to provide detailed pathways for diversion detection.

At the University of Tennessee Knoxville Dr. Steve Skutnik developed CYclus-Based ORiGen (CyBORG) [12]. This module expands the reactor analysis capabilites of Cyclus by coupling with Origen. The extension adds reactor data libraries that allow users to perform origen reactor depletion calculations within Cyclus. Other higher fidelity models include the Bright-lite package created at the University of Texas Austin by Dr. Erich Schneider and Dr. Anthony Scopatz [13]. This package adds a medium fidelity reactor, fuel fabrication facility, and reprocessing facility modules.

1.2.2 Pyroprocessing

Pyroprocessing is an electrochemical separation method used primarily for metallic fast reactor fuel. This reprocessing technique uses molten salt, whose composition differs depending on the facility. Molten salt such as LiCl-KCl has a broader stability range compared to water, allowing high potentials to be used for separation. In aqueous reprocessing, separation would be conducted in a nitric acid and water medium. This becomes a problem when chemically isolating heavier elements such as lanthanides and actinides. Controlling the oxidation states of these elements often requires potentials outside the stability of water. Increasing a potential beyond the medium's stability (or electrochemical window) limits oxidation and reduction [14]. Hence, pyroprocessing was born to improve non-proliferation and reprocessing capabilities.

In addition to the improved redox control of heavier elements, we co-extract materials of interest so they cannot easily be refined for weapons. This is done through the electrorefining and electrowinning stages by separating a pure uranium stream as well as a uranium/transuranic (U/TRU) mixed stream. The U/TRU can then be readily used for fuel fabrication while maintaining proliferation resistance.

Electrochemical separation is the driving force behind pyroprocessing. Electrochemistry relies on the use of Gibbs free energy to determine the required amount of energy to drive a reaction forward.

Figure 1.1 demonstrates an electrochemical process that generates electricity as a basic example. The processes described here follow the same principles but require energy to run. As shown in this basic example, ions are exchanged between the anode and cathode in an attempt to balance the potential difference. In the case of pyroprocessing, the potential difference is driven by an external source of electricity. An anode and cathode are used to force the desired ions to deliver charge from one end of the cell to the other. These ions

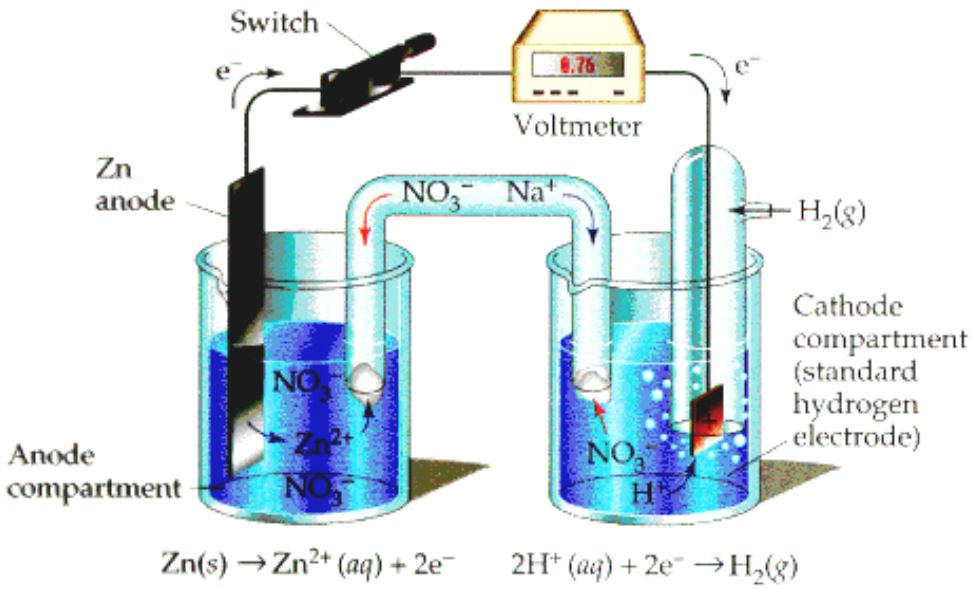

Figure 1.1: Basic example of movement of ions within a galvanic cell, sourced from [15].

collect on the surface of the cathode can then be separated from the rest of the solution. By controlling the voltage of the system as well as the composition of the anode, cathode, and electrolyte we can ensure the removal of unwanted elements/isotopes.

Voloxidation

Voloxidation follows the chopping and decladding of the spent fuel. The process is very similar to annealing with regards to materials. The uranium dioxide is heated to temperatures around 700-1000°C which allows gases and some fission products to escape the fuel pellet, as well as convert UO_2 to U_3O_8 [16]. Voloxidation, in most cases, takes place in air which provides plenty of oxygen for oxidization of solid UO_2, which has the chemical balance [17]:

$$3UO_2 + O_2 \rightarrow U_3O_8$$

The above reaction relies on the expansion of uranium at elevated temperatures. A positive feedback is also established: as the uranium dioxide converts to yellowcake powder, the fuel element expands, exposing more uranium dioxide to oxygen. The rate of this reac-

tion/conversion depends on the temperature and gas used. Higher temperatures will yield a faster reaction rate; even 500 $°C$ is sufficient for 99% removal in 4 hours.

An added benefit of running a pyroprocessing voloxidation sub-process at the temperatures previously mentioned, 700-1000$°C$, is the removal of gaseous fission products, as shown in Figure 2.3. The Pyroprocess Integrated inactive Demonstration facility (PRIDE) at KAERI takes it a step further and voloxidates at 1250$°C$ to remove troublesome fission products at the beginning of the cycle[16]:

Voloxidation temperature	H-3	C-14	Kr-85	I-129	Cs	Tc	Ru	Rh	Te	Mo
1 250ºC	100	100	100	100	98	100	100	80	90	80

Figure 1.2: Voloxidation separation stream composition at 1250 $°C$, units shown are % mass separated.

As shown in the table above, pyroprocessing begins with removing a majority of high activity isotopes are removed from the system protecting equipment and personnel. These gases are sent to an off-gas treatment facility that makes use of various scrubbing techniques such as liquid scrubbing, cyrogenic distillation (for removal of Kr), and caustic scrubbing [17].

Electroreduction

Following off-gassing and conversion to yellowcake, the non-metallic fuel must be converted and reduced to a molten salt mixture, this is called electrolytic reduction or electroreduction. In most cases this is done with a LiCl-KCl salt eutectic combined with a Li_2O catalyst. The electrolytic reduction phase consists of three main parts: UO_2 recovery, reduction, and rare earth (RE) removal.

The chemical balance for an anode and cathode in a LiCl-KCl salt is as follows:

$$UO_2 \rightarrow UO_2^{2+}(LiCl - KCl) + 2e^{2-} \qquad anode$$

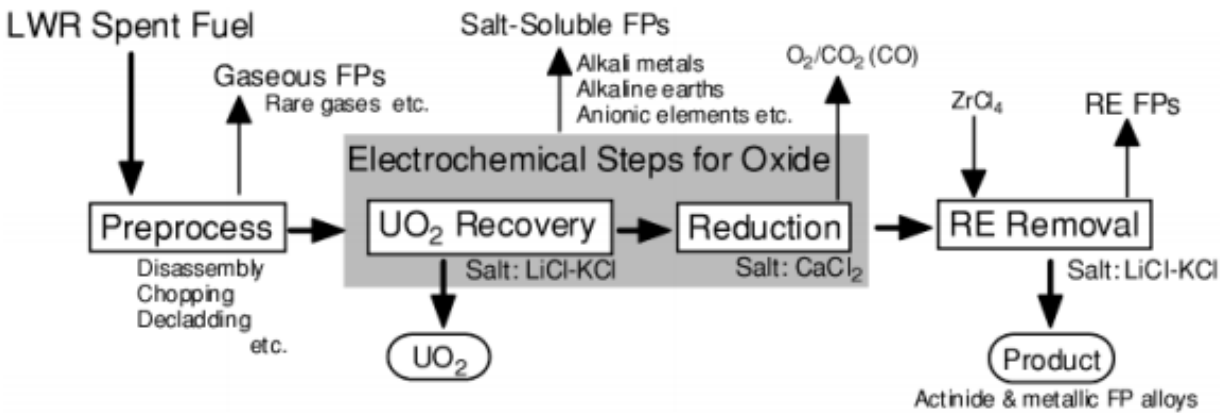

Figure 1.3: Electroreduction flow sheet [18].

$$UO^{2+}(LiCl - KCl) + 2e^{2-} \rightarrow UO_2 \qquad cathode$$

As in other separations technologies, noble metals can often follow the uranium through the rest of the process. The lurking noble metal fission products (FPs) cause an increase in radioactivity of the UO_2 stream. Therefore, the weight percent dissolution of uranium is critical in reducing the amount of noble metal FPs that follows to the product stream. Lithium oxide can also be used as a catalyst to draw uranium to the cathode while leaving the noble metal fission products in the salt. This is done with 1-3wt% Li_2O in the following equations [19]:

$$Li_2O \rightarrow 2Li^+ + O^{2-}$$

$$UO_{x/2} + xLi \rightarrow U + xLi_2O$$

These equations make a continuously driven loop dragging uranium (either UO_2 or U_3O_8) from the anode to the cathode. Disassociated lithium ions from the first equation break apart the uranium and oxide, with help from the electric potential. The uranium collects on the cathode while the Li_2O is recycled and drives the first equation forward again. Reduction then occurs on the cathode where the U, TRU, rare earths, and noble metals (NMs) have collected. This is achieved by evolving oxygen gas along the anode using the following

reactions[19, 16]:

$$Li^+ \rightarrow Li + e^- \qquad Cathode$$

$$M_xO_y + 2yLi \rightarrow xM + yLi_2O \qquad Cathode$$

$$O^{2-} \rightarrow 0.5O_2 + 2e^- \qquad Anode$$

Electrochemical reduction results in an alloy of reduced uranium, transuranics, rare earths, and noble metals; however, we want to minimize the amount of rare earths and noble metals in the product. The RE FPs can be removed from the alloy by substituting another chloride into the LiCl-KCl eutectic. Ohta et al. explored the use of $ZrCl_4$ as this substitue which changes the chemical balance to the following [18]:

$$3ZrCl_4(LiCl - KCl) + RE \rightarrow 3Zr + 4RECl_3(LiCl - KCl)$$

Yakamura demonstrates this process to have a decontamination factor of 10 with regard to separating REs from actinides [20]. Additionally, by using Zr as the metal substitute, it is compatible with fuel fabrication later [18].

Electrorefining

Electrorefining is the primary process in pyroprocessing, and is the first stage for fast reactor fuel, since metallic fuel does not require reduction or chopping. In addition to being the most important process, it is also the most complex with a multitude of input parameters and material streams. The goal of the refining process is to separate the uranium and TRU from the alloy ingot formed in the reduction phase. Two streams will be formed for the fabrication of fuel: one stream that is a mix of U/TRU at the desired ratio, and the other a pure stream of uranium. The refining efficiency relies on temperature and current primarily, however, advanced methods are being developed. KAERI, for example, has investigated

adding a central stirrer, lowering pressure, and rotating the anode [8]. The rotation aims to mix the uranium in the salt such that none gets stuck on the bottom or edges of the vessel. Stirring too vigorously, however, can lead to the removal of uranium dendrites from the cathode thereby decreasing efficiency.

The governing reactions that allow this process to work are based on the stability constants and oxidation potential of the remaining FPs. The voltage used, 0.5-1V, is such that uranium is unstable in the chloride form [16], while TRUs have a higher stability. This leads to TRU remaining in chloride form, along with some uranium, and pure uranium accumulating on the cathode. The chloride reaction follows the below equation, and will run to the right as long as there is uranium within the salt [16].

$$UCl_3 + TRU(RE) \rightarrow U + TRU(RE)Cl_3$$

$$UCl_3 + 3Na \rightarrow 3NaCl + U$$

$$UCl_3 + 3Cs \rightarrow 3CsCl + U$$

$$UCl_3 + Pu \rightarrow PuCl_3 + U \qquad \delta G = -22.44kcal$$

$$4UCl_3 + 3Zr \rightarrow 3ZrCl_4 + 5U \qquad \delta G = 31.123kcal$$

As shown by the reactions above, the TRU have a negative Gibbs free energy value for spontaneous reactions while the transition metals do not [21]. This leads to the transition metals remaining in the anode basket while the TRU are drawn into the liquid cadmium cathode [22].

Electrowinning

The electrorefiner accumulates TRUs and rare earth fission products within the salt. These isotopes build up and require separation and disposal, therefore the salt from the refiner

is sent to the electrowinner. This stage further purifies the salt by targeting the electric potential of TRUs, RE, and U again [22, 16]. Placed in liquid cadmium once again, the three groups have overlapping electric potentials leading them all to deposit in the cadmium [22]. While the refiner's role is to generate a stream of pure uranium, the electrowinner performs co-extraction of uranium and TRUs. This inherent proliferation resistance is a main draw of the pyroprocessing technique. Rare earths are still present on the cadmium and further separations must be conducted. These elements are removed through the addition of $CdCl_2$ which oxidizes the rare earths, while the uranium and TRUs are unaffected. These oxidized elements fall back into the salt, leaving the purified U/TRU stream on the electrowinner.

Although the facility is great in terms of safeguards, pyroprocessing has its share of drawbacks as well. Currently, pyroprocessing can only be performed as a batch process, which significantly limits throughput compared to a continuous facility. Additionally, the safety and economic concerns of running a molten salt plant are much greater than a nitric acid one. Despite these downsides, pyroprocessing is an efficient use of electrochemical separation and a leader in proliferation resistant separations.

ANL, INL, and KAERI, among other entities, have produced pyroprocessing facility designs. In order to encompass a broad range of flowsheets, we must take a generic approach when modeling pyroprocessing. Accordingly, this work includes the following sub-processes: voloxidation, electroreduction, electrorefining, and electrowinning. While electrorefining is the process of primary concern, each of the processes has an important role.

1.3 Goals

This work aims to generically model a pyroprocessing facility with medium fidelity, appropriate for simulating diversion scenarios. Modeling this within Cyclus enables us to explore the capability of modeling sub-facilities and diversion. In addition, we use this higher fidelity model to verify transition scenarios such as EG01-EG24 within Cyclus [3]. Finally we

aim to identify impactful facility parameters for various facility layouts through sensitivity analysis.

Chapter 2

Methods

This chapter outlines the modeling choices made when designing a pyroprocessing facility. The framework a model resides in is a key design choice, and we cover why Cyclus provides a productive environment for designing and testing this facility. In the Cyclus framework we design the Pyre archetype as a generic modular facility using material balance areas and identifying key signatures and observables. Leveraging this information, we design a diverter class to integrate within Pyre. This diverter tracks and alters operational parameters to mimic the actions of shadow fuel cycles.

2.1 Cyclus

Cyclus is a modular, agent-based nuclear fuel cycle simulator that models the flow of material through user-defined nuclear fuel cycle scenarios. Cycamore, the CYClus Additional MOdules REpository, provides common facility archetypes (separations, enrichment, reactor, etc.) [23]. The Cyclus framework provides benefits compared to other fuel cycle simulators, some being the open source nature, modular capabilities, and use of agents. Customizable agents populate simulations, allowing for a diverse use case. Exact isotopes are dynamically tracked between facilities in discrete time steps [2]. Isotope tracking is a key aspect of Cyclus that we will use for signatures and observables, in addition to allowing burn-up calculations in more complex fuel cycle scenarios.

2.1.1 Open Source

Many fuel cycle simulators have restrictive licenses such as ORION, VISION, or COSI. This restricts nuclear fuel cycle simulator use and development in academia, therefore a tool such as Cyclus fills a necessary gap. The Cyclus framework relies on free libraries and open development that allows continuous contributions from various universities and fields of research. This increased accessibility allows more diverse use and expansion of the simulator as seen with codes like CyBORG and Bright-Lite [12, 13].

2.1.2 Reproducibility

Cooperation and collaborative development are a major part of open source development. This is maintained through code reviews. These reviews are conducted by peers, and are used to check code style, documentation, and functionality. As such, any addition to open source code in particular should be well tested for bug detection, verification, and confidence in results. Thorough testing allows concurrent or future developers to maintain and expand the project while ensuring all capabilities are maintained. Following these guidelines, we implement a number of tests verifying trade capability and sub-process physics to ensure reproducibility. The details of these verifications will be explained further in Chapter 3.

2.1.3 Modular

The modularity of Cyclus also contributes to the customizability of fuel cycle scenarios. Rather than having locked material connections between facilities, the modular Cyclus framework allows easy implementation of new connections. This is handled through the use of a dynamic resource exchange (DRE) in the Cyclus kernel [24]. The DRE uses a system of material offers and requests to find the best connections at each time step. Figure 2.1 demonstrates how the agent API is used to mediate the Cyclus kernel DRE and the implementation of each agent.

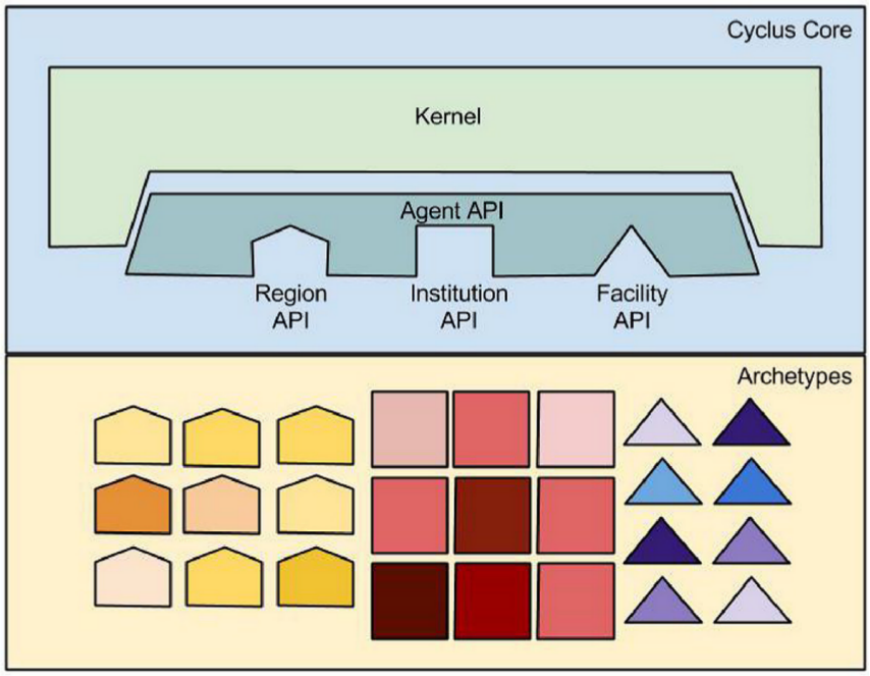

Figure 2.1: Visualization of the CYCLUS API for modular facilities, regions, and institutions [2].

The structure seen in Figure 2.1 is largely responsible for the potential breadth of agent types of varying fidelity. Provided new agents have the appropriate material trade offers and requests, facilities can be designed to any required fidelity.

2.1.4 Archetypes

Agents contain a hierarchy of *regions, institutions, and facilities* such that *regions* hold one or more *institutions*. Similarly, *institutions* control *facilities* necessary for the actual fuel cycle. For this work, we are most interested in the implementation of *facilities* - particularly how they are defined. Nuclear fuel cycles contain multiple variations of the same facility requiring a diverse collection of pre-designed facility process models, known as *archetypes*. These archetypes are used to define the physics and behavior of specific facility types such as reactors, reprocessing, enrichment, etc. Archetypes with pre-defined parameters are referred to as prototypes (an AP1000 for example is a prototype). Furthermore, facilities are prototypes that have been given specific data such as deployment time, location, lifetime,

etc.

2.2 Pyre

This thesis work included original design and implementation of Cyclus facility archetype, Pyre, which has various capabilities. Pyre was designed such that multiple potential pyroprocessing facilities can be modeled at medium fidelity. To accomplish this, and improve upon the lower fidelity of the separations archetype found in Cycamore, Pyre separation efficiencies is informed by higher fidelity models including SSPM and AMPYRE [25, 5]. The below Figure 2.2 incorporates material balances for each sub-process and highlights some key parameters Pyre requires the user to provide in the input file or monitor for diversion.

2.2.1 Structure of Pyre

The Pyre archetype separates each sub-process (voloxidation, electroreduction, electrorefining, and electrowinning) to be handled independently, letting the user determine which aspects are necessary for their facility. Pyre takes this approach to improve handling of various waste streams. Ceramic waste must go through the electroreductor, whereas metallic fuel can go straight into the electrorefiner [7]. This reduces reprocessing time, as Pyre does not force redundant processes.

Governing Pyre Class

The archetype treats each sub-process as optional and independent, letting the user determine which aspects are necessary for their facility. Each sub-process handles its own diversion and material tracking. The streams produced from these processes are sent further through the facility, and the streams are recorded. Waste streams are used to verify nominal operation before being traded to a storage facility. Product streams are further refined by each sub-process until the fuel fabrication stage. The pure uranium stream and U/TRU

stream are then offered up for trade with a fuel fabricator.

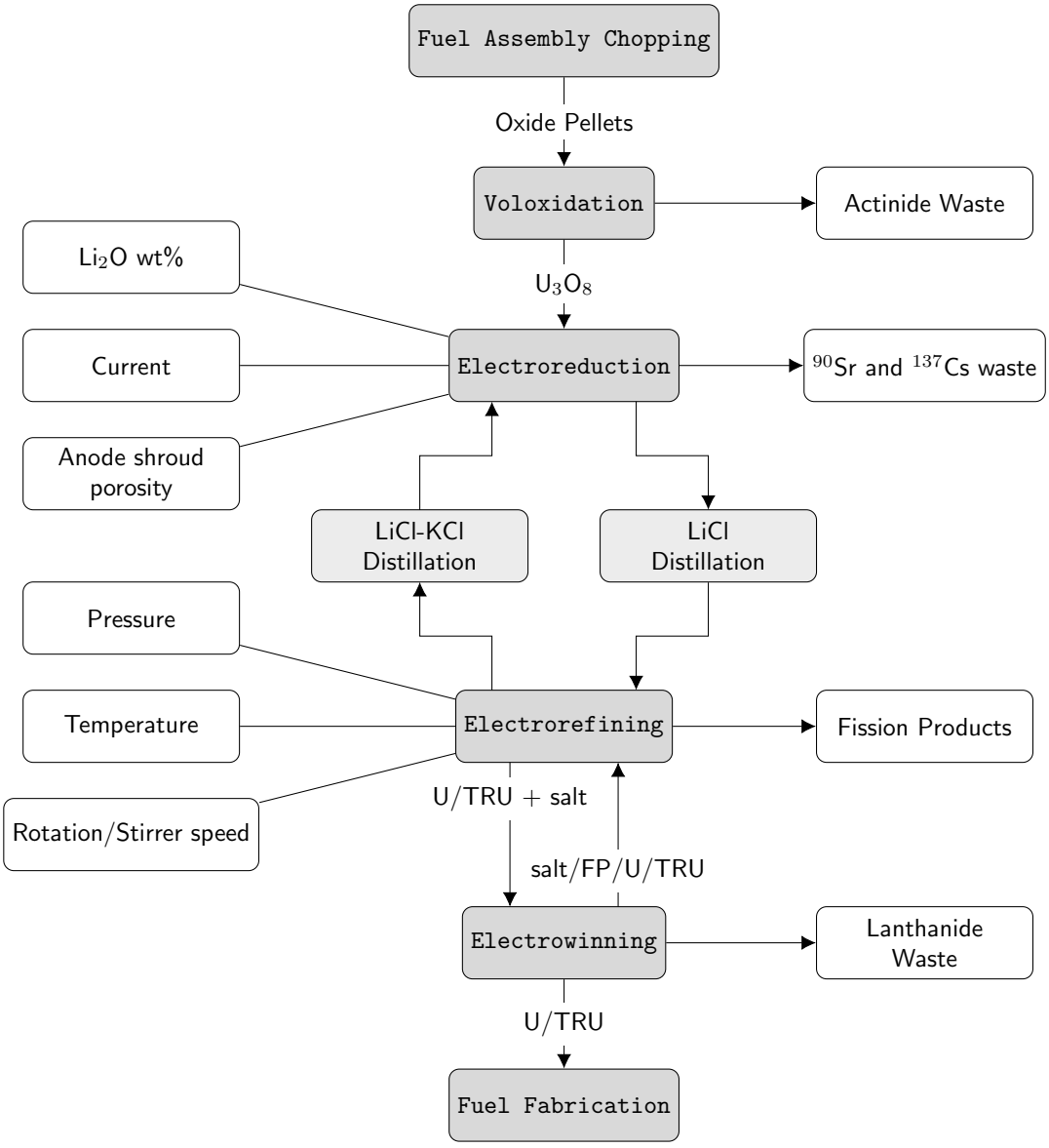

Figure 2.2: Pyre material flowchart [6].

2.3 Signatures and Observables

Before constructing a pyroprocessing archetype, appropriate signatures and observables must be determined to set as our input parameters. To identify signatures and observables found

in a variety of pyroprocessing plants, we expand upon what was discussed in chapter 1 by looking at experimental data from electrochemical plants. The primary resources are from INL, KAERI, and ANL [22, 26, 7, 27]. We break up these signatures and observables into two distinct categories: direct and indirect, corresponding to signatures and observables, respectively. If the inspector has direct access to material these are referred to as signatures, whereas, indirect monitoring, such as power draw or thermal imaging, represent a lower level of access.

Potentially trackable signatures and observables include truck deliveries and power draw [28, 29]. This list is expanded upon in Table 2.1 to include pyroprocessing parameters. For this work we narrow down the list to more facility specific parameters rather than observables like the parking lot or truck movement. We also use this table to determine the most common operational settings such as temperature, pressure, current and flow rate.

2.3.1 Material Balance

In order to improve material accountancy, points where material is transfered need to be monitored through material balance areas. We take a material balance area over each sub-processes using the signatures and observables identified in Table 2.1. These balance areas are shown through flowcharts describing operational parameters in green, and signatures and observables in red.

Voloxidation

Light Water Reactor (LWR) fuel must be treated and separated before proceeding with electrochemical processes. Uranium dioxide heated to 500°C is converted to U_3O_8 while noble gases, carbon, and tritium are collected to decay in storage. Actinides are also converted to their stable oxide forms and a majority are removed [26, 17]. Heating uranium dioxide above 800°C increases voloxidation throughput. Cycling oxidants between H_2 and air also improves the U_3O_8 reaction rate [17].

Sub-process	**Parameters**	**S & O**	**Refs**
Voloxidation	Volume	Tritium	[17]
	Oxidant	^{14}C	[26]
	Flow Rate	^{129}I	
	Temperature	^{85}Kr	
	Time	Actinides	
Electroreduction	Volume	^{90}Sr	[6]
	Batch Size	^{135}Cs	[26]
	Li_2O wt%	^{137}Cs	[30]
	Current	Power Draw	[22]
	Porosity	Shipments	[31]
	Distillation Speed	Throughput	
	Time		
Electrorefining	Volume	Fission Products	[32]
	Time	Power Draw	[22]
	Material	Waste Salt	[26]
	Anode Rotation	Vacuum Pressure	[33]
	Stirrer Speed	Temperature	[34]
	Pressure	Throughput	
	Temperature		
Electrowinning	Current	Power Draw	[26]
	Shroud Material	Cadmium Waste	[22]
	Time	Fission Products	[6]
	Flow Rate	Lanthanides	
		^{135}Cs	
		^{137}Cs	
Facility	Throughput	Shipments	
	Batch Size	Parking Lot	
		Thermal Image	

Table 2.1: Archetype inputs and signatures & observables at each sub-process.

Figure 2.3 shows the material balance of the voloxidation process which can be translated to an equation for material unaccounted for (MUF):

$$\sigma_{MUF} = UO_2 - Gases - Ac - Tritium - U_3O_8 \tag{2.1}$$

Red boxes correspond to losses while the only gain is chopped UO_2 as described previously. Each of these variables can be detected through signatures and observables, monitoring

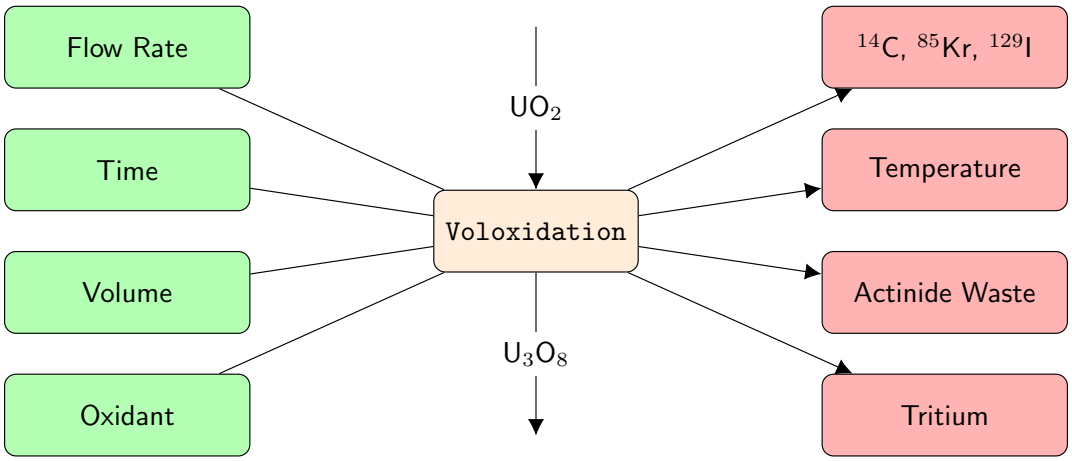

Figure 2.3: Voloxidation material balance area [17].

temperature and waste for example can inform efficiency.

Electroreduction

Yellowcake, created in voloxidation, enters the cathode, a negatively charged metal basket. A current density between 100 and 500 mA/cm^2 is applied to the anode in a molten LiCl salt. The electrolytic reduction process primarily results in diffusion of Cs, Ba and Sr, along with reduction and conversion of Zr into metallic form [30, 26]. Electroreduction can further improve its throughput by adding Li_2O as a catalyst; this catalyst also prevents dissolution of the anode [30]. Since Li_2O is used to speed up the reaction, the operators could add more oxide than reported to International Atomic Energy Agency (IAEA). More frequent shipments of lithium oxide can be tracked as an observable to match records.

Translating Figure 2.4 to an equation for MUF yields the following:

$$\sigma_{MUF} = U_3O_8 - X_{^{90}Sr} - X_{^{137}Cs} - X_{U+LiCl} + X_{LiCl} \tag{2.2}$$

The electroreductor primarily prepares fuel for use in the electrorefiner, therefore few materials are removed. Notable signatures include the ^{90}Sr and ^{137}Cs and power draw

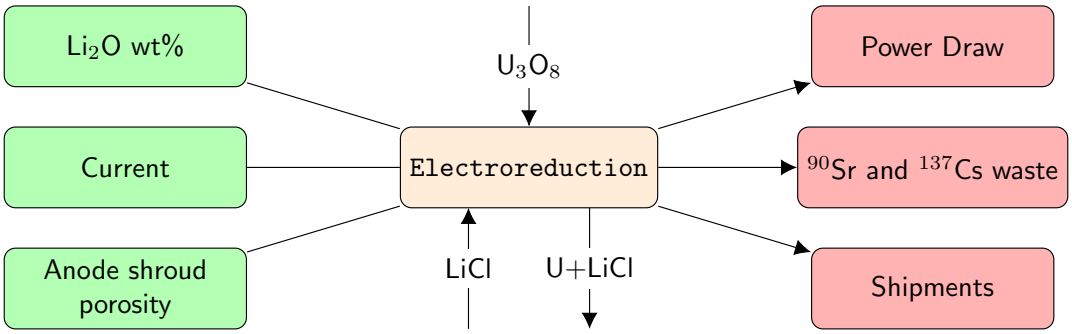

Figure 2.4: Reduction material balance area [32].

associated with changing current.

Electrorefiner

Once in metallic form, electrorefining electrochemically separates uranium and TRUs for fuel fabrication. The uranium and salt mixture from reduction is fed into an anode basket suspended in a graphite cathode. A LiCl-KCl eutectic is used as an electrolyte above 500°C [26, 22]. Uranium dissolves at the anode to recombine at the cathode as metallic uranium. Waste TRUs and lanthanides are in a soluble chloride form while fission products and cladding remain in the anode basket. Finally, actinides and fission products are removed from the cladding electrochemically [22].

Lee et al. [32] show decreasing system pressure improves removal efficiency experimentally. Temperature, however, exhibits the opposite effect: as temperature decreases so does salt removal. This comes into effect particularly depending on instrumentation and containment material choice [32]. Iron, for example, limits operating temperature because a eutectic forms at 725°C [35]. In facilities where iron equipment is present, temperatures are limited to 700°C, hindering efficiency.

$$\epsilon = aT^3 + bT^2 - M + c \tag{2.3}$$

$$M = \frac{\alpha P_{eq}}{\sqrt{2\pi mRT}} \tag{2.4}$$

Where

$\epsilon =$ efficiency

$M =$ evaporation rate

$\alpha =$ evaporation coefficient

$P_{eq} =$ equilibrium pressure

$m =$ molecular weight

$T =$ temperature

$a, b, c =$ coefficients derived from experimentation

Cathode arrangement and anode rotation speed also affect the collection of uranium dendrites [32].

$$\epsilon = 0.032\omega + 0.72 \qquad \omega < 1 \tag{2.5}$$

$$\epsilon = 0.03log(\omega) + 0.84 \qquad 1 < \omega < 100 \tag{2.6}$$

Where

$\epsilon =$ efficiency

$\omega =$ rotation speed

The above is combined into the flowchart seen in Figure 2.5 where key inputs are highlighted in green and wastes or signatures appear in red.

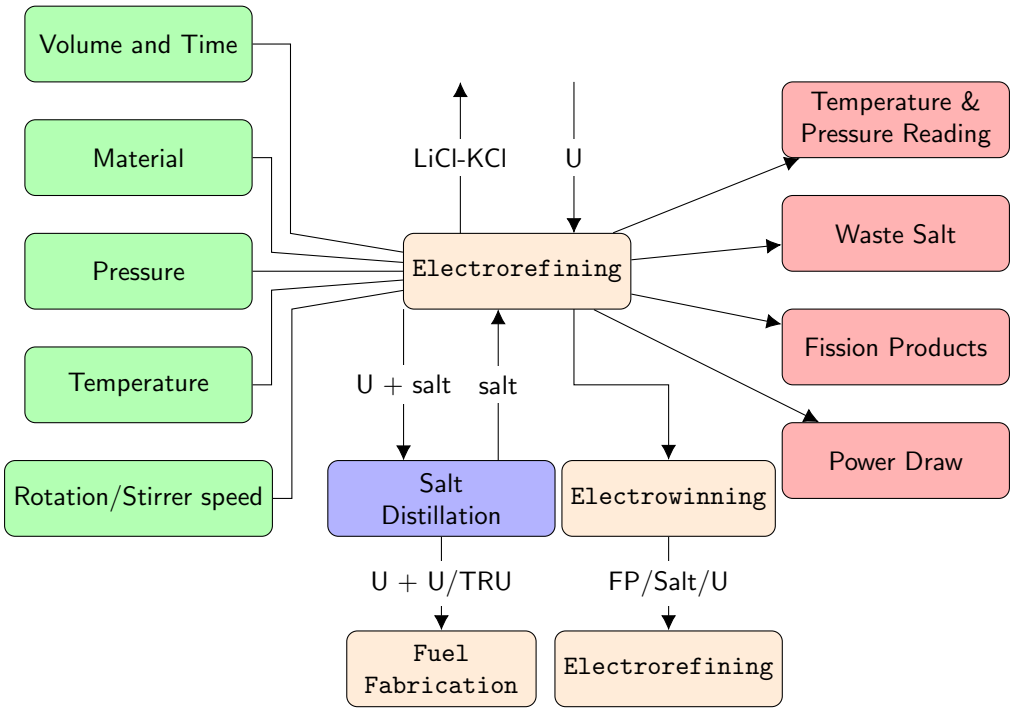

Figure 2.5: Refining material balance area [32].

The electrorefining process also produces a fission product waste stream which requires monitoring. The following products are produced and tracked in Pyre at this step: Tc, Ag, Pd, Rh, Ru, Mo, and Zr [26]. Uranium and transuranic (TRU) product streams separated at this stage are sent to fuel fabrication, while the remaining salt is reformed as an oxidant and recirculated. Separation efficiencies are taken after recirculation and treated as a once-through cycle.

$$\sigma_{MUF} = X_{Uin} + X_{salt} - X_{LiCl-KCl} - X_{ws} - FP - X_{Uout} \tag{2.7}$$

Where

$$X_{ws} = \text{waste salt quantity}$$

The MUF equation for the electrorefiner is generalized by equation 2.7 to account for the numerous fission products and actinides removed in this stage. This process contains the first product stream shown in the MUF, and signatures and observables increase accordingly. The increased complexity of the electrorefiner leads to additional parameters and material streams to monitor. Pyre leverages these additional signatures using the equations discussed above to monitor the behavior of the electrorefiner.

Electrowinner

Molten salt containing TRUs from electrorefining is separated through electrowinning. This process separates trace uranium quantities, lanthanides and fission products. At 500°C there is approximately 99 wt% reduction in actinides and lanthanides [26]. Throughput also depends on material choice for the inert electrodes, impacting separation efficiency [33]. A shroud surrounds the anode to provide a path for O^{2-} ions to the anode and prevent Cl_2 from corroding the anode [34, 30]. Optimum operating current depends on material choice for the anode shroud since a nonporous shroud limits ion pathways to the anode contact points. Higher porosity corresponds to free ion paths and a higher current. Increased currents reduce the separation time for electroreduction and electrowinning [30]. The following equation describes the effect of current on material separation, however η_s is gathered experimentally [36]:

$$\frac{dm}{dt} = (1 - \eta_s) I \frac{M}{3F} \tag{2.8}$$

Where

$$m = \text{mass}$$

$$\eta_s = \text{sticking coefficient}$$

$$I = \text{current}$$

$$M = \text{molecular weight}$$

$$F = \text{Faraday's constant}$$

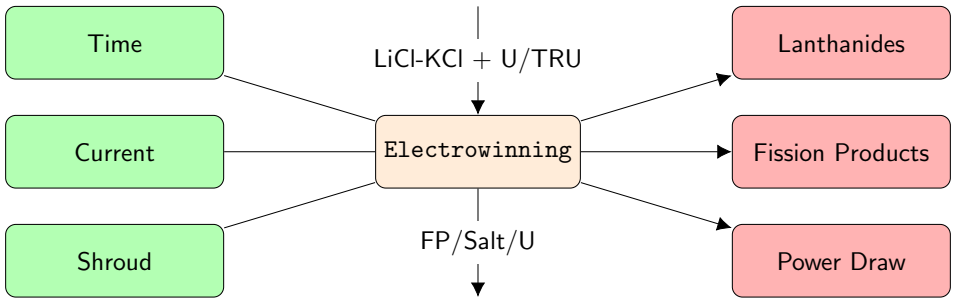

Figure 2.6: Winning material balance area.

The above information and flowchart correspond to the following MUF equation.

$$\sigma_{MUF} = X_{LiCl-KCl+U/TRU} - X_{FP/salt/U} - X_{Ln} - X_{U/TRU} \tag{2.9}$$

Waste from the electrorefiner is sent to the electrowinner in the form of LiCl-KCl+U/TRU where the U/TRU stream is removed for fuel fabrication. Additionally, lanthanides and actinides are removed before recycling the salt to the electrorefiner for further reprocessing. This process results in the following signatures and observables for tracking in Pyre: current, reprocessing time, and decay of FP.

2.3.2 Waste Forms

Waste from pyroprocessing plants exists in three main waste streams in which IAEA can directly measure their *signatures*. Monitoring signatures require direct access to the waste streams. These techniques vary depending on the waste form. Leading approaches include non-destructive assay, multiplicity counting, and a plutonium to curium ratio measurement [37, 38].

Diverter

Figures 2.7 and 2.8 shows the difference between nefarious diversion and operator diversion. In Figure 2.7 nefarious diversion occurs through the shipment, and can be detected by a discrepancy in shipment records. These diversions do not require access to the facility, only that a bad actor can siphon from or steal a shipment. The more difficult case to handle, shown in Figure 2.8, imagines an inside man altering operational settings to increase product over reported quantities. Normal operation can be seen in gray and can be difficult to detect diverted material using shipment methods as with nefarious diversion. The scenario we are concerned with is operator diversion; we wish to determine the most important points in the plant to monitor for potential diversion. A side effect of this goal is that we must be able to detect diversion by changing key operational settings.

Figure 2.7: A flowchart demonstrating the process of nefarious diversion.

Cyclus does not natively handle diversion from inside facilities as required for the goals for Pyre. We implemented a higher fidelity diversion model through the diverter class to

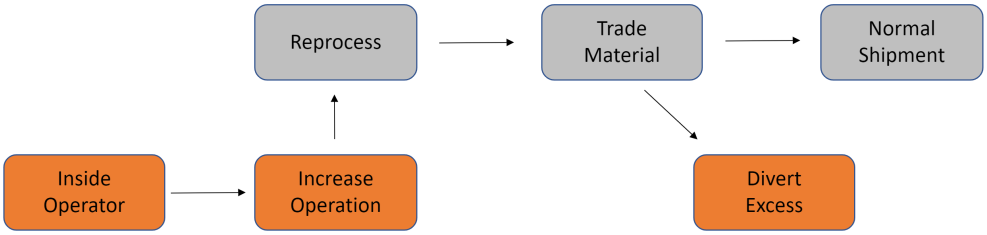

Figure 2.8: A flowchart demonstrating the process of operator diversion.

handle operator and nefarious diversion. This class is specific to the Pyre archetype currently, as the diversion facility must be set up to allow it. The diverter class' goal is to inform the Pyre facility what parameters are being changed to divert material. The algorithm used for this can be seen in Figure 2.9 which inputs the sub-process that contains an inside man, the parameters he has access to, and how much material he wishes to divert. The diverter directs this information to the appropriate sub-process which then uses a bisection function to determine the parameter value associated with the new product.

2.3.3 User Input

Pyre, as with all Cyclus archetypes, is fully configurable through the text-based input file. The input consists of the operational settings shown in Table 2.1 and the separation efficiency for each isotope. The efficiency input for each sub-process corresponds to that facility's ideal state. Operational settings act as a capacity factor, reducing the overall efficiency to match those seen in test facilities. This input structure allows users to follow predefined example facilities, or input their own separation efficiencies. As a result of this work, input files for PRIDE, INL, and ANL based facilities have been generated. However, a user can also input their own parameter relationship equations if those provided do not accurately reflect their facility model.

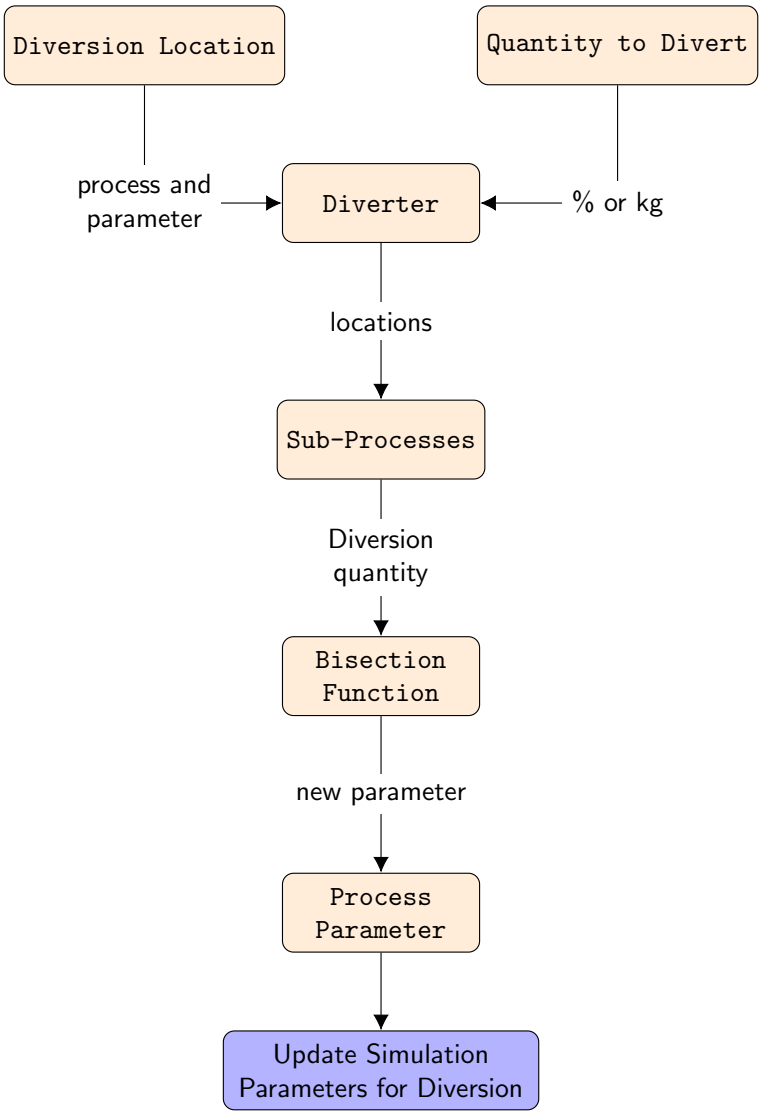

Figure 2.9: Pyre diverter class flowchart.

Chapter 3

Simulating Fuel Cycles

3.1 Simple Verification

In this work, several demonstration simulation verified the capabilities implemented in Pyre. Cyclus archetypes are expected to meet a number of capabilities such as trading, decommissioning, and isotope tracking. To demonstrate these functionalities we ran a simple scenario with one source, sink, and Pyre facility. The Pyre facility is run at default values corresponding to an average installation. The source facility provides light water reactor (LWR) SNF with a composition given by Duderstadt [39].

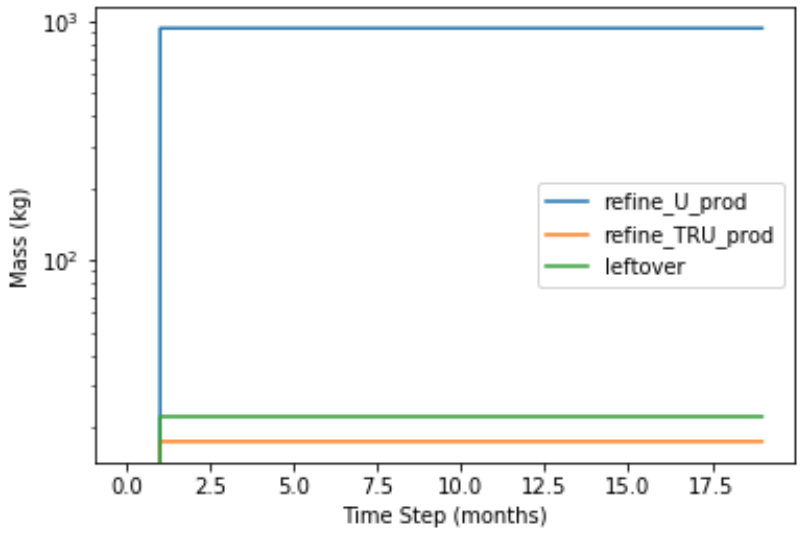

Figure 3.1: Product time series of a simple simulation.

The above Figures 3.1 and 3.2 track the shipment of the LWR SNF from the Pyre facility to the `sink`. Individual waste streams are identified and verify the functionality of each sub-

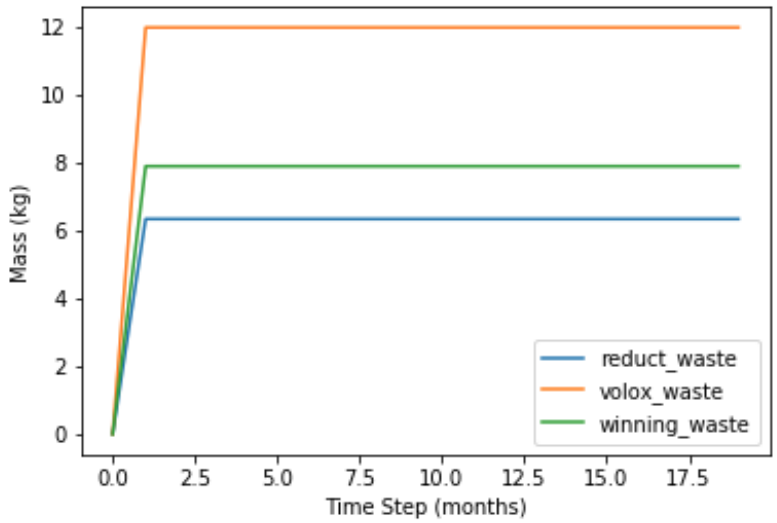

Figure 3.2: SNF in the Pyre facility for the simplest simulation.

process in this LWR configuration. Since the scenario was run with constant sub-process parameters and a constant number of facilities, the transactions are expected to remain constant and the above figures meet this expectation. In addition to demonstrating sub-process capabilities, material transactions with other Cyclus facilities can also be observed as expected. Material trade is verified by the continual separation of SNF without a buildup of waste or product.

3.1.1 Isotopic Streams

Another key aspect of material transactions is the composition of each shipment. To meet Cyclus standards Pyre must be able to track each isotope and trading with various facilities. This is done two ways within Pyre: monitoring waste and product transactions, and tracking isotopic compositions. Figure 3.3 compares three waste streams isotopically. This comparison further illuminates the performance of each sub-process by confirming the appropriate separation of elements. The electrowinner, shown in green, correctly contains heavier elements such as lanthanides while the electroreductor, in red, is responsible for the lighter metals as well as changing oxidation states which is not reflected in these streams.

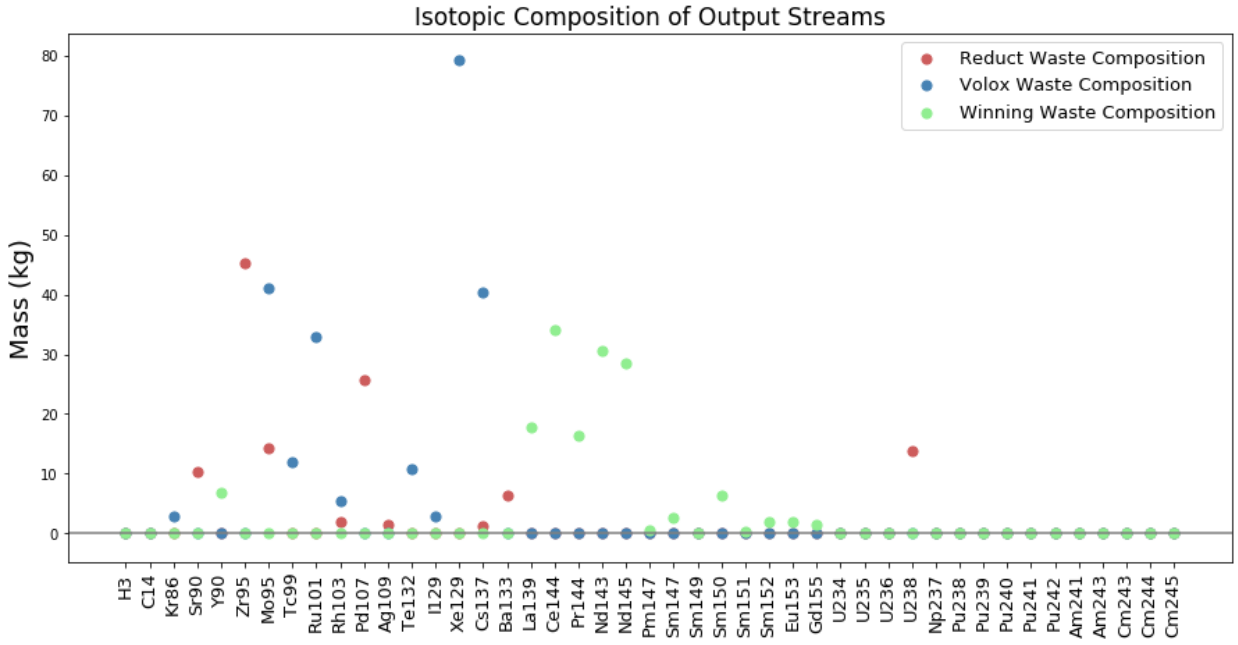

Figure 3.3: Isotopic Composition of Average Waste Streams

3.1.2 Simple Diversion

Simple diversion cases are handled through two example scenarios. The first scenario describes a facility that operates at a higher than reported current, leading to increased power draw. The second case imagines a facility diverting as much material as possible by reporting a low efficiency and operating at optimal levels. Figures 3.4 and 3.5 are used to demonstrate these simple diversion scenarios. In particular, the scenario run for Figure 3.4 compares a facility of default values with one of increased power draw. Increasing the power draw of the facility affects sub-process currents. Separation efficiency of the electroreductor and electrowinner is improved by increasing the current in the anode resulting in the material unaccounted for (MUF) shown above. Despite no change, the voloxidation stream remains to confirm only appropriate processes are being affected.

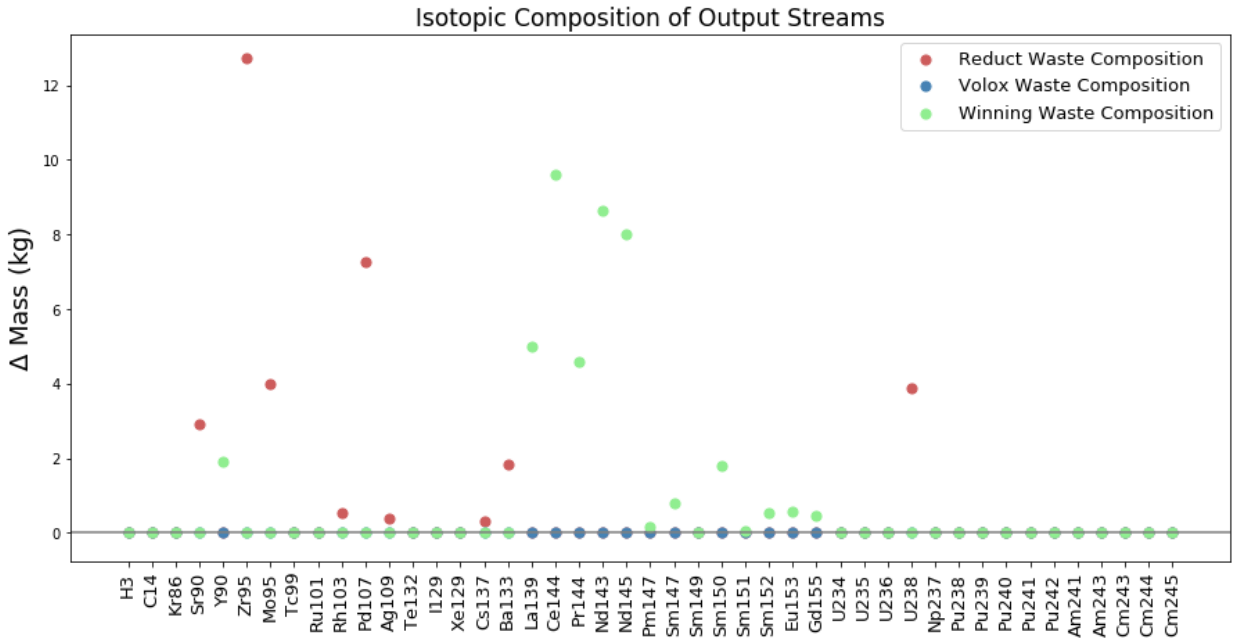

Figure 3.4: Isotopic Composition of Current Diverted Waste Streams

3.1.3 Maximum Diversion

The other diversion case explored here is a theoretical maximum diversion scenario in which two scenarios are run: where parameters are set to their maximum and minimum values respectively. Although unrealistic since diversion is easily detected, the scenario shows us the worst case and can be used to inform inspection intervals. Figure 3.5 shows that after a 20 month scenario, approximately a significant quantity of plutonium is unaccounted for. As such, inspections would need to occur at a similar interval, depending on the reported capacity.

3.2 US Fuel Cycle Transition

After testing the capabilities of Pyre in a steady state scenario, we implemented the archetype in the EG01-EG24 transition scenario described in the goals of this work.

Table 3.1 shows the setup for a sodium fast reactor (SFR) transition. In addition to the above information, the scenario is initiated with 200 LWRs with another 200 being deployed

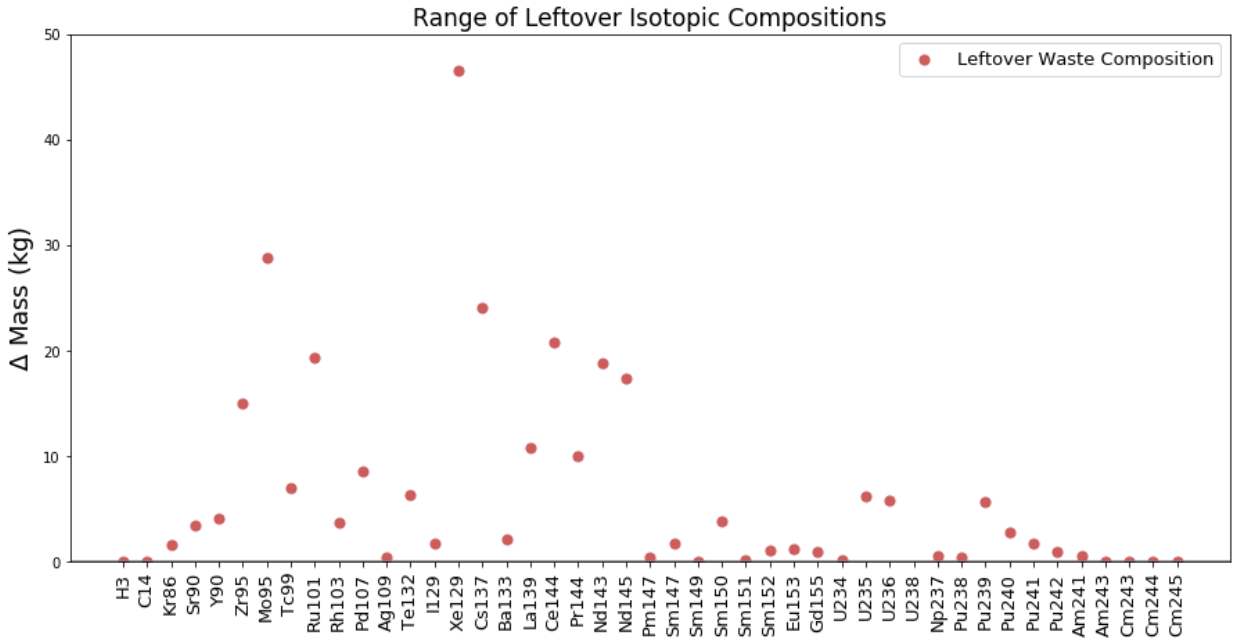

Figure 3.5: Range of Isotopic Values for maximum potential diversion.

in 2015 at the transition period. Two Pyre prototypes are deployed to handle the different fuel types seen in the above scenario. The PRIDE-based facility is configured to reprocess ceramic LWR waste while the INL-based facility handles metallic SFR fuel, and is deployed after the transition.

Figure 3.6 demonstrates the deployment and decommissioning of reactors in this scenario. In order to meet the average 1% annual power growth, additional reactors are necessary while appropriate SFR fuel quantities are accumulated.

3.2.1 Pyre Performance

To verify functionality of the Pyre archetype we observe the fuel production and utilization. Figures 3.7 and 3.8 demonstrate the appropriate reprocessing and fabrication of SFR fuel. Figure 3.7 shows the SFR pyroprocessing plants begin producing a sustainable amount of fuel around year 2125. Since all SFRs are breeders in this scenario, we can see that as more reactors are deployed the TRU stock increases exponentially at year 2150. Similarly, the overall utilization of uranium improves as reprocessing is heavily used. Improved uranium

Details	Value	Unit
Simulation start	1959	years
Simulation end	2215	years
LWR Lifetime	60	years
50% of LWRs	80	years
Transition start	2015	years
Reprocessing Facility	PRIDE Pyre	–
New LWR lifetime	80	years
SFR Lifetime	80	years
SFR breeding ratio	1.014	–
Reprocessing Facility	INL Pyre	–

Table 3.1: Transition Scenario setup and details.

utilization corresponds to the closing of the nuclear fuel cycle. The demand for uranium mining and milling diminishes as the SFR population grows causing an increase in uranium effectiveness. This is further exemplified in Figure 3.7 which illuminates the shift from enriched uranium based fuel to a TRU mix.

Figure 3.9 illustrates the complete transition from LWRs and UOX fuel to SFRs at year 2180. As seen in Figures 3.7 and 3.8, TRU fuel production has increased enough to self-sustain the next generation of SFR reactors and decommission remaining LWRs.

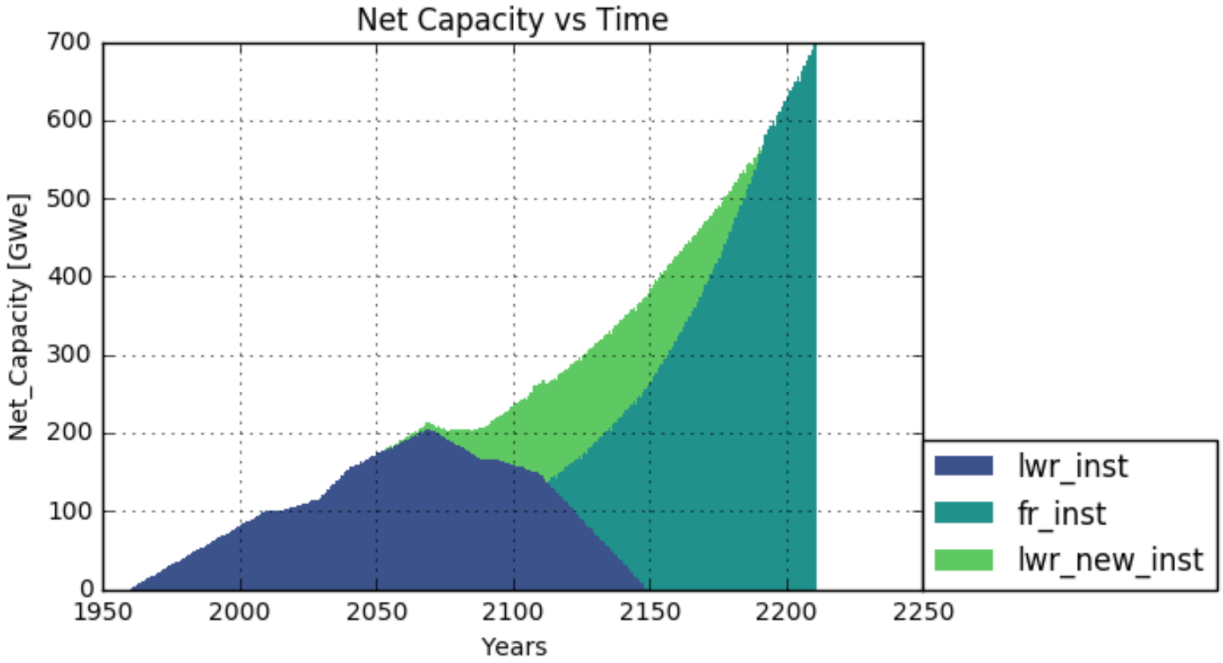

Figure 3.6: Net Power Capacity over Time

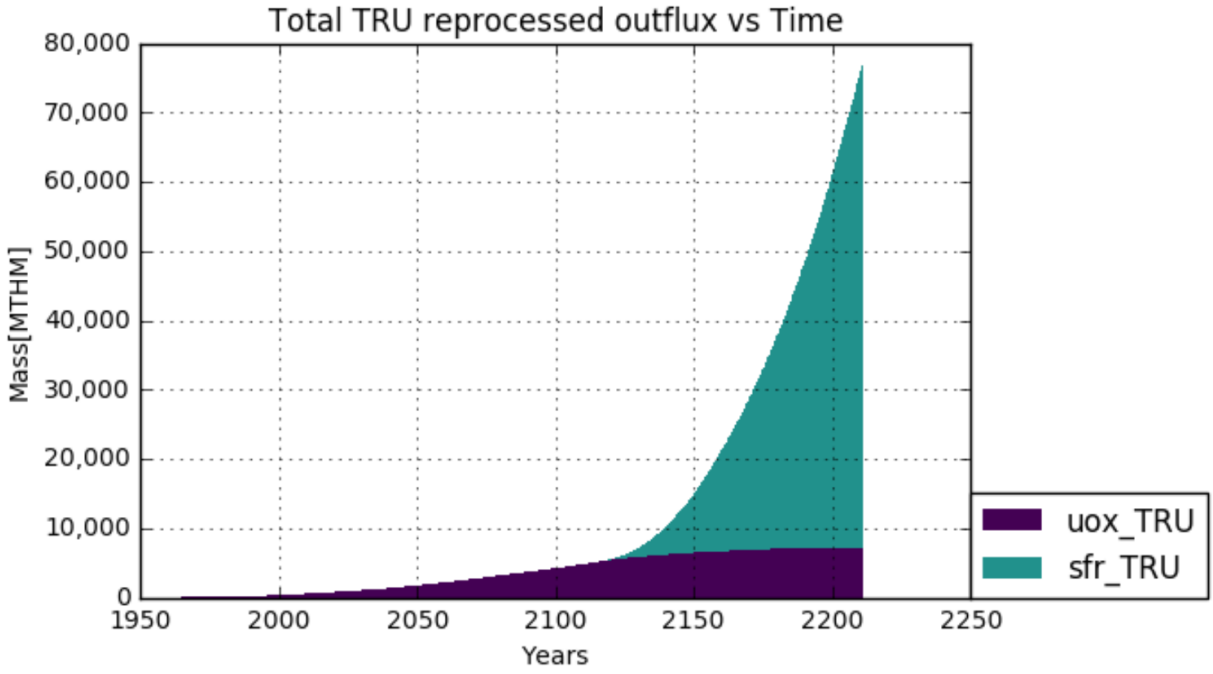

Figure 3.7: TRU utilization over time in EG01-EG24 transition scenario.

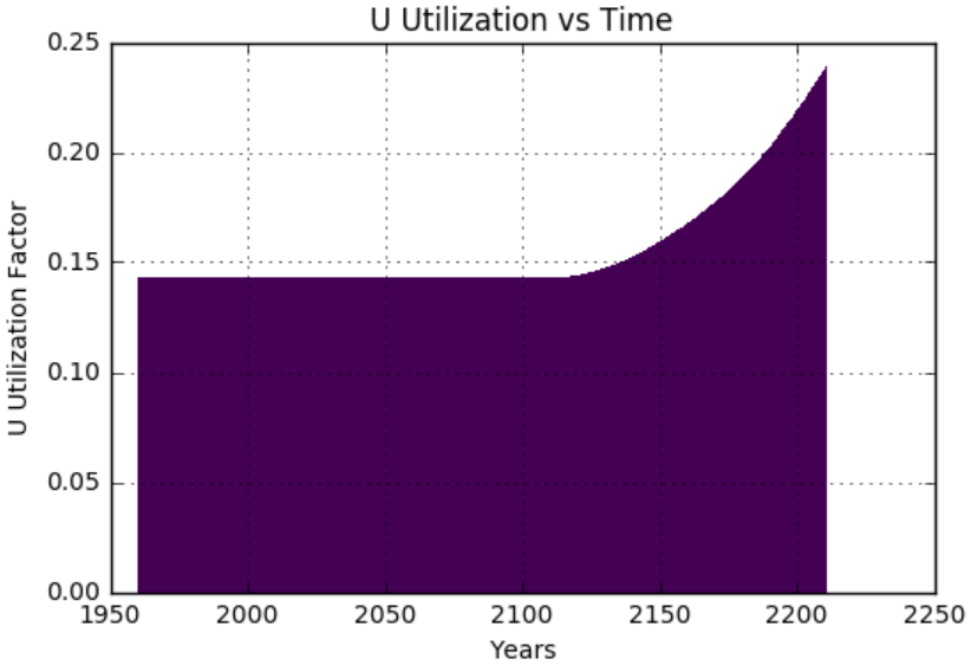

Figure 3.8: Uranium utilization over time in EG01-EG24 transition scenario.

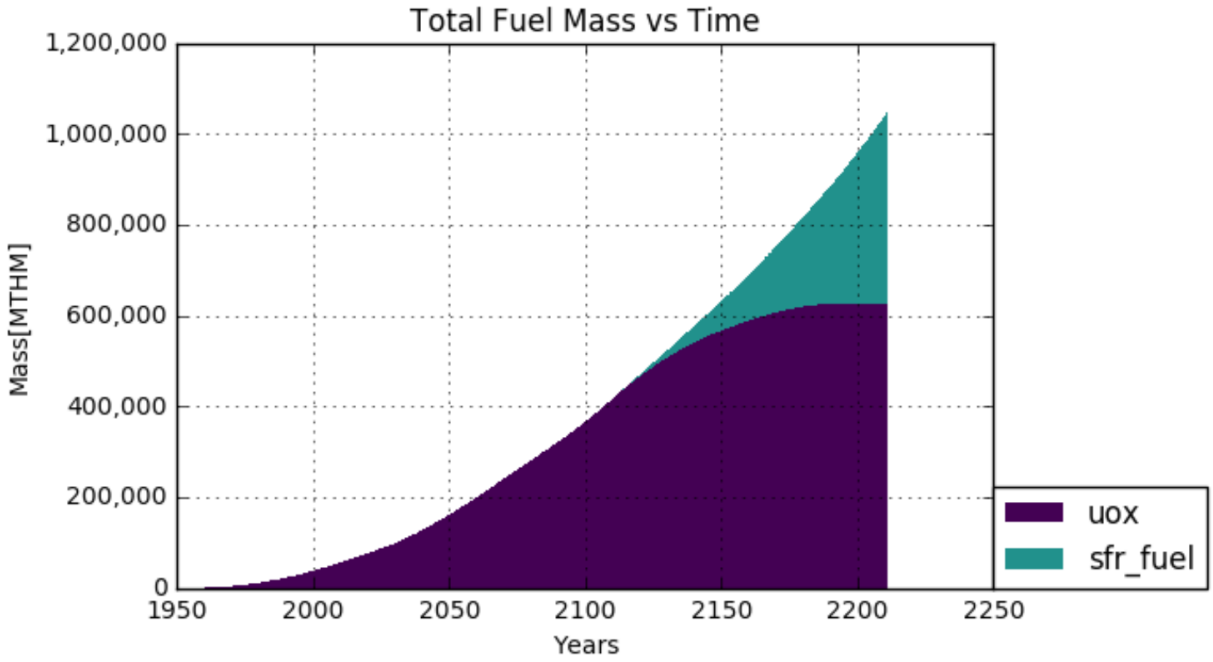

Figure 3.9: Mass of fuel types over time in EG01-EG24 transition scenario.

Chapter 4

Diversion Detection

The second aspect of this work identifies locations sensitive to diversion in a generic pyroprocessing facility. This work leverages two approaches: applying a cumulative sum detection algorithm and performing sensitivity analysis on key facility parameters.

4.1 Cumulative Sum

4.1.1 Requirements of Diversion Detection

The cumulative sum method (CUSUM) applied to Pyre was chosen to fit the following requirements: function with minimal prior information, have online diversion detection capabilities, and fit a modular approach. The CUSUM change detection algorithm calculates expected mean value of an observed data stream as shown by the following equations [40].

$$f_{t+1} = max(0, f_t + x_t - \mu - \delta) \tag{4.1}$$

Where

$x_t =$ observed data at time t

$\mu =$ approximated mean of x

$\delta =$ acceptable change

This general function adds new observed values to the calculated mean. If the value is within a region of allowable change, typically 3σ, the change is not reported. We favor this online diversion detection capability in an effort to achieve timely detection goals set by the IAEA [4]. These intermittent inspections only have access to portions of the complete data stream, thus we aim to mimic reality as closely as possible. In addition, we need this algorithm to work on a variety of facilities with various active sub-processes.

4.1.2 Limitations of selected method

The CUSUM approach is not without its drawbacks: since there is no prior data assumed we must generate a reasonable mean from observed data before being able to detect diversion. In this work we assume a startup time of approximately 6 months before an appropriate mean can be developed. The next limitation faced with this approach is that CUSUM assumes one can only observe one data stream at a time, while real inspections take a wide range of conditions into account. This concern is addressed by using sensitivity analysis, as seen later in this chapter, to inform on the most crucial sub-processes or settings.

CUSUM relies on a variable mean and noise to obscure possible change points. When a simulator knows the exact value at each time step, without human reporting or measurement error, change detection becomes trivial. To best represent the uncertainty inherent in material accountancy measurement, noise is artificially created when the CUSUM class reads data. This way Cyclus retains its constant operating value while the change point has potential to be obscured by measurement error. These detector uncertainties are assumed from common non-destructive and destructive assay practices used by the SEE LANL safeguards training course [41].

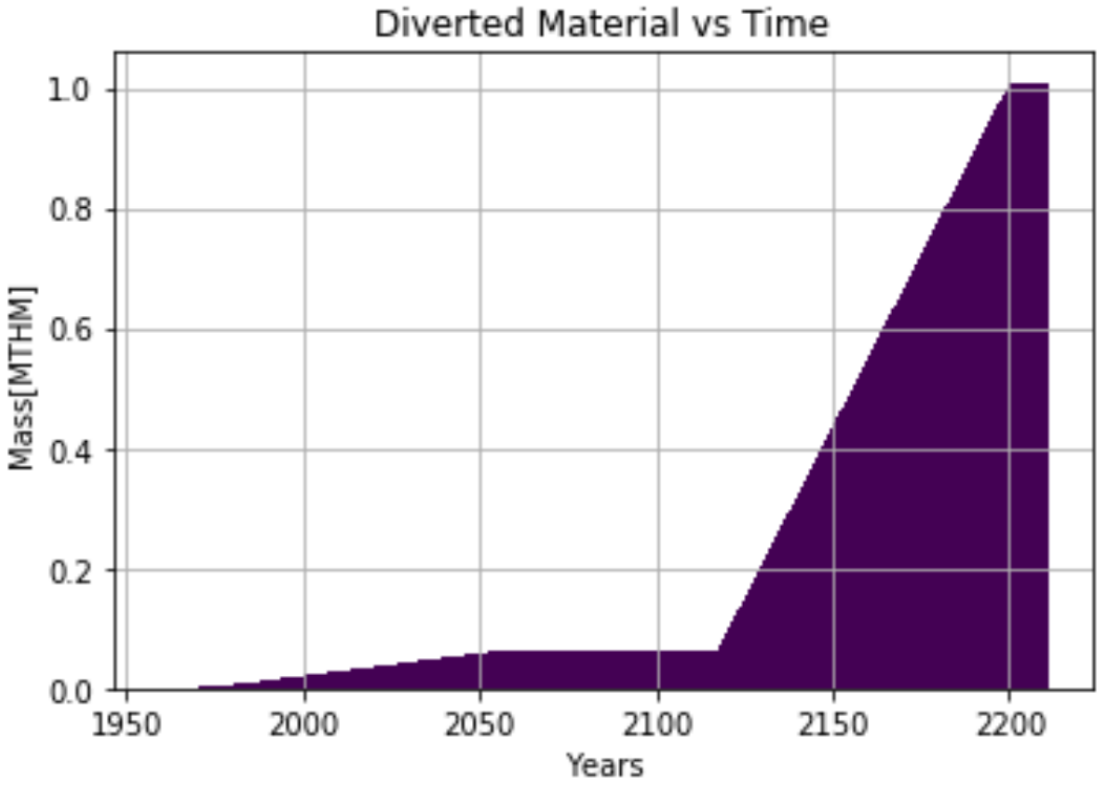

Figure 4.1: A timeseries of diverted material from transition scenario EG01-EG24.

4.2 Verification

To test operator diversion capabilities, we ran the EG01-EG24 transition scenario shown in chapter 3 with inside operators. The scenario described in Table 3.1 contains an LWR and SFR configuration for Pyre. Each prototype siphoned material with different quantities and frequencies to demonstrate its reconfigurability. The pyroprocessing facility that exclusively accepts LWR fuel siphoned off 5% every 10 timesteps while the facility that only accepts SFR fuel siphoned off 1% excess every other timestep. Results for this scenario are shown in Figure 4.1. This plot verifies the customization of the diverter class, demonstrating multiple configurations within the same simulation. This capability is integral in capturing diversion in complicated shadow fuel cycles containing multiple pyroprocessing prototypes.

4.3 Sensitivity Analysis

The sensitivity analysis approach in this work illuminates the limits of monitoring future pyroprocessing facilities. This work relies on Dakota to alter Cyclus input files and provides a number of statistics packages, allowing us to easily run batches of scenarios. To properly use Dakota with Cyclus, we must use DCWrapper, which uses python to interface between Dakota and Cyclus' xml input files. Key parameters were sampled over a range of values for diversion to verify the archetype's capabilities and identify operational ranges. The range for each parameter is shown in Table 4.1.

Parameter	**Lower Bound**	**Upper Bound**	**Units**
Electrorefiner Temp	750	1000	$°C$
Electrorefiner Pressure	100	760	mTorr
Electrorefiner Stirrer Speed	0	100	rpm
Electrowinner Current	5	10	Amps
Electrowinner Flow Rate	2	4.5	cm/s
Electrowinner Process Time	1	4	hours

Table 4.1: Range of Each Sensitivity Analysis Parameter Sample.

Parameters were selected from the most attractive sub-processes for diversion, the electrorefiner and electrowinner. These two processes are responsible for the production of Uranium and U/TRU ingots, therefore sensitivity analysis was run on each of their key parameters: Temperature, Current, Flowrate, Pressure, Stirrer Speed, and Reprocessing Time. Six samples were selected at regular intervals across the range of each parameter. For each setting we observe how much material can be diverted within a month.

4.3.1 Electrorefiner Temperature

The first setting for consideration is the electrorefiner's temperature. As discussed in methodology, the range for this setting is 500 to 1000 $°C$ with typical operation above 750 $°C$. These values can be seen isotopically in Figure 4.2. The 750 $°C$ stream is then subtracted from the sampled streams to determine the impact of increasing temperature on divertable material.

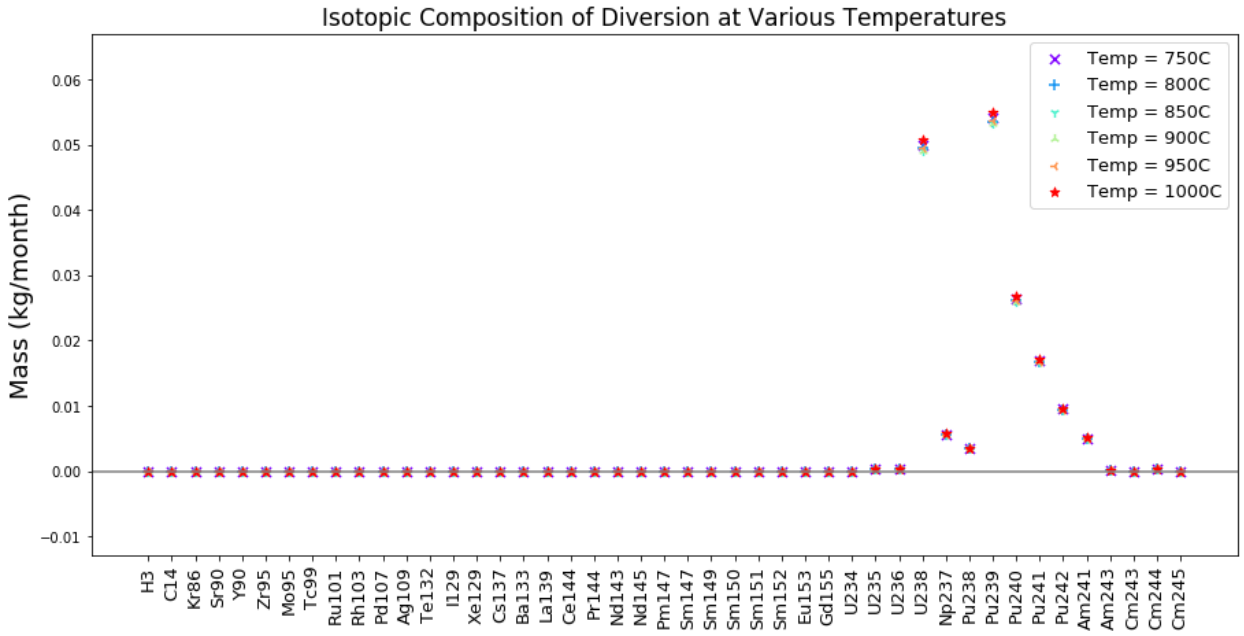

Figure 4.2: Isotopic composition of the diverted material stream at various electrorefiner temperatures.

While temperature is a key aspect to the electrorefiner, Figure 4.3 shows that temperatures approaching 1000 $°C$ result in diminishing returns.

4.3.2 Electrorefiner Pressure

Available in advanced electrorefiners, lower vacuum pressure can improve separation efficiency as well. Similar to our analysis of temperature, isotopic compositions of divertable material can be seen in Figure 4.4. Our baseline for the comparison is atmospheric pressure as this will represent facilities lacking this functionality. Figure 4.5 compares the five other samples to atmospheric pressure. This further illuminates the plateau separation efficiency experiences in relation to pressures lower than 364 mTorr.

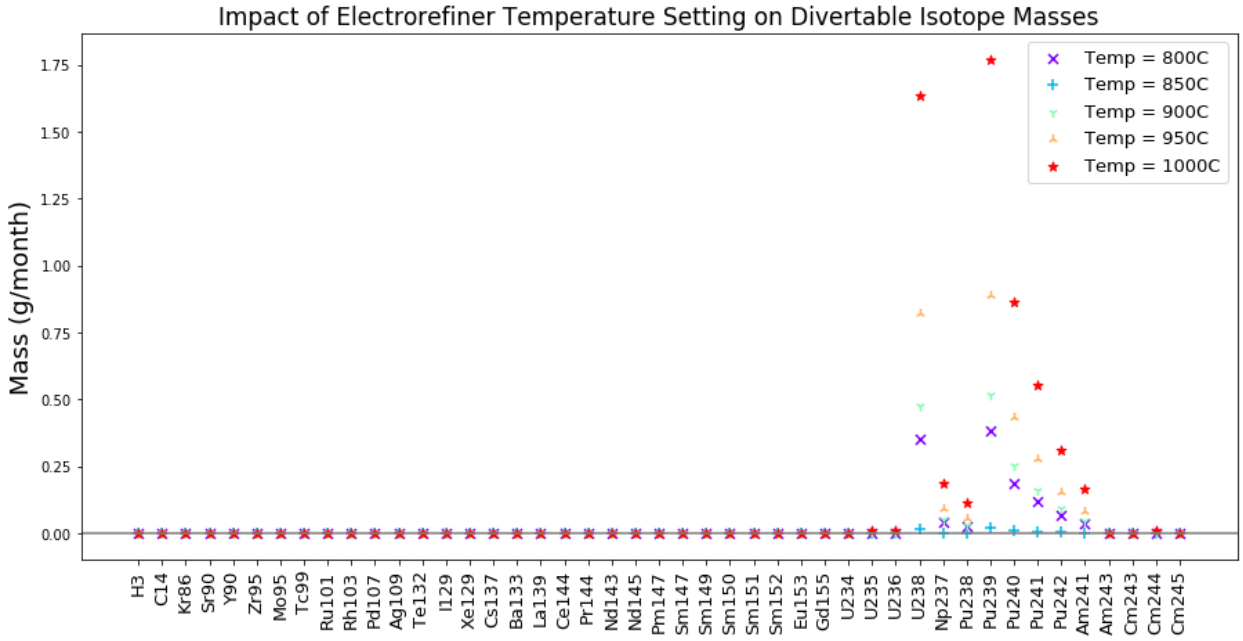

Figure 4.3: Isotopic composition of the diverted material stream at various electrorefiner temperatures.

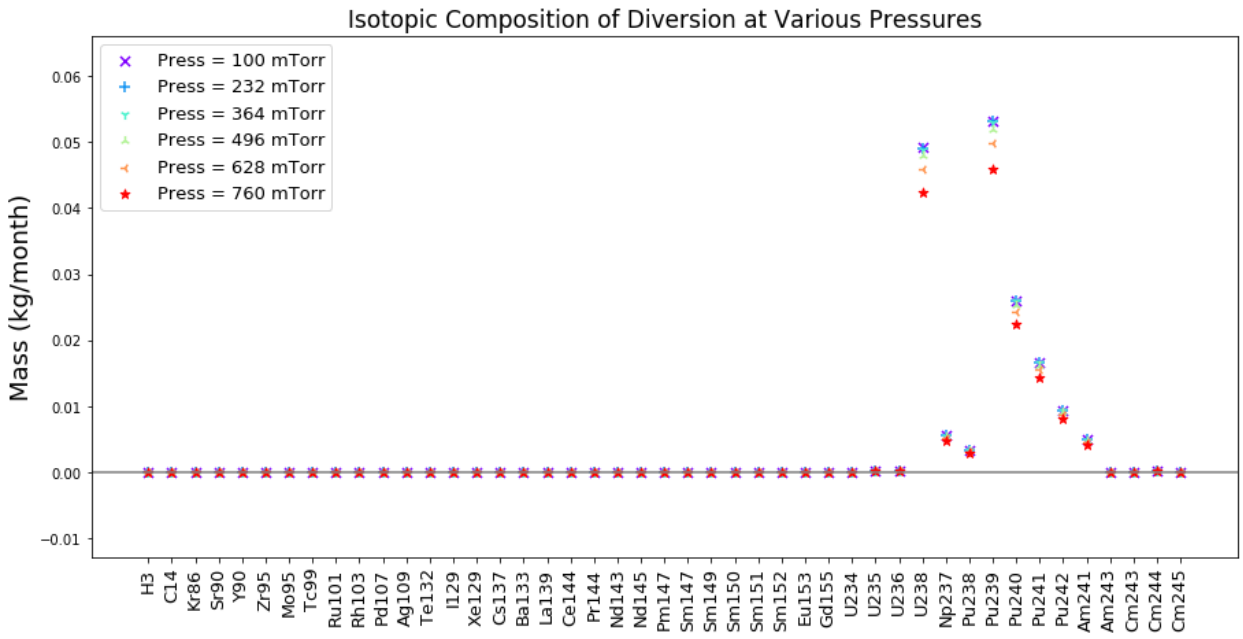

Figure 4.4: Isotopic composition of the Diverted material stream at various electrorefiner pressures.

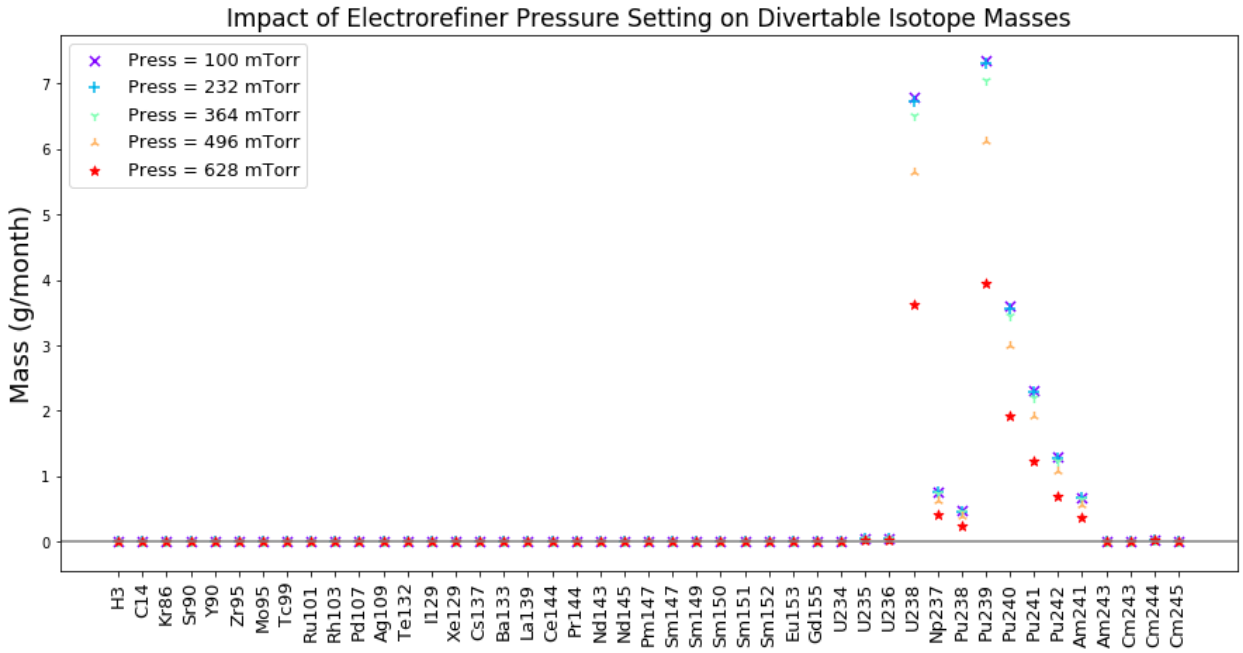

Figure 4.5: Isotopic composition of the Diverted material stream at various electrorefiner pressures.

4.3.3 Electrorefiner Stirrer Speed

The central stirrer is another setting particular to advanced refining techniques [32]. Pyre tracks this parameter since adding a stirrer to processes can be a simple procedure. Figure 4.6 shows the isotopic distribution associated with a range of different stirrer speeds. Stirrer speed higher than 100 rpm results in uranium dendrites returning to the salt. Therefore, in Figure 4.7 this work took 0 rpm as our baseline to represent facilities with no stirrer, and 100 rpm as our maximum.

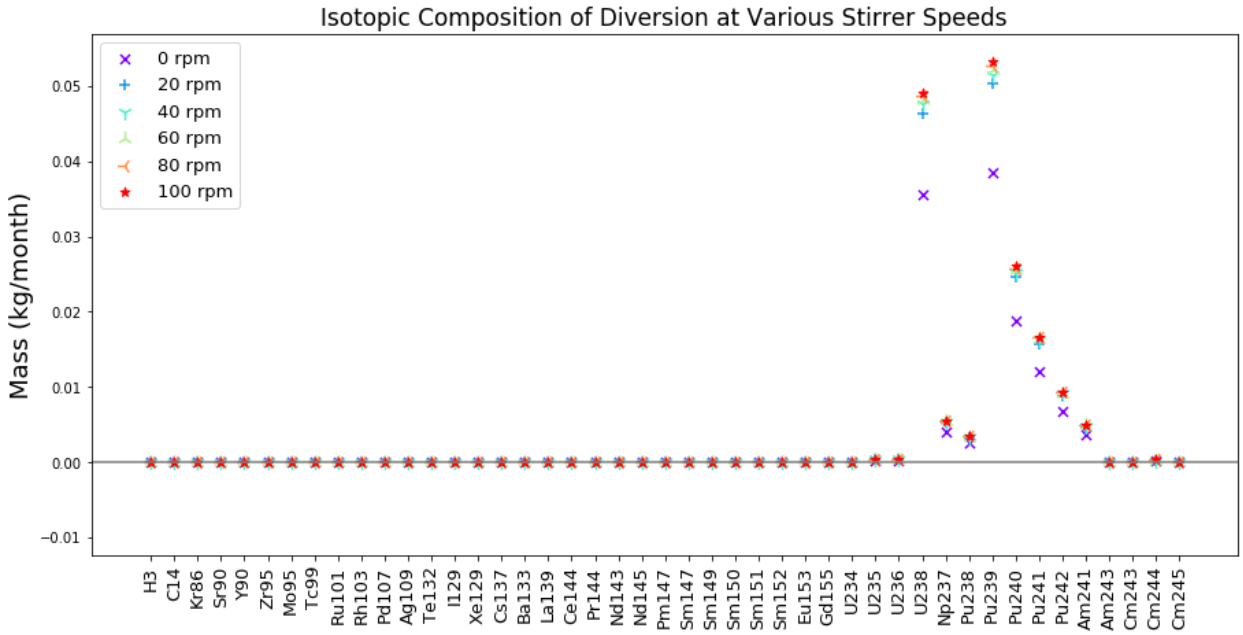

Figure 4.6: Isotopic composition of the diverted material stream at various central stirrer speeds.

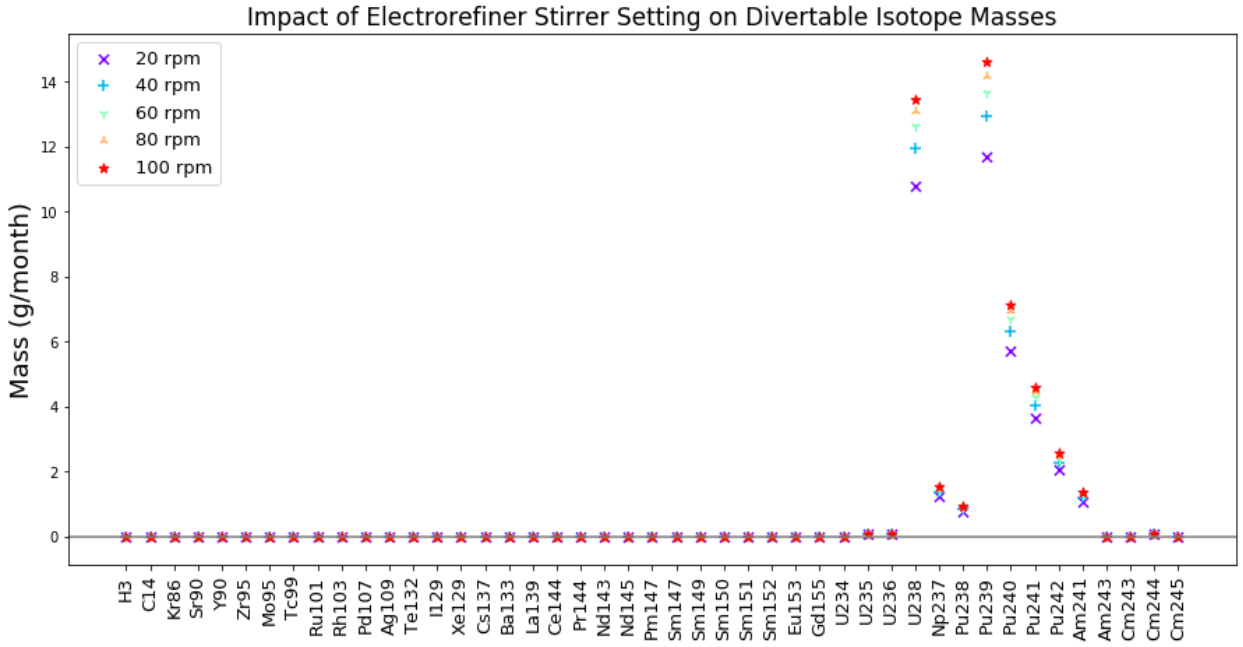

Figure 4.7: Isotopic composition of the diverted material stream at various central stirrer speeds.

4.3.4 Electrowinner Current

The primary setting for the electrowinning sub-process is the current. The current's relationship with efficiency decreases in separation beginning around 10 A. This is seen in Figures 4.8 and 4.9 as 10 A is below the efficiency of 5 A. This relationship occurs due to increasing voltage no longer aiding in separation of some lanthanides as described in chapter 2. Figure 4.9 shows that the key operating range lies within 6-8 A.

4.3.5 Electrowinner Flow rate

Similar to the central stirrer of the electrorefiner, increasing the flow rate through the electrowinner can aid removal of additional lanthanides and TRU. Flow rates shown are linear rates, with the bounds corresponding to minimum and maximum values tested in experimental facilities. Figures 4.10 and 4.11 demonstrate a steady increase in removal rates with increasing flow.

4.3.6 Electrowinner Reprocessing Time

The final setting we chose to observe was time spent in the electrowinner. We chose this sub-process since it is closely related to the U/TRU product stream. Comparing Figure 4.13 to Figure 4.11, we can see that increasing reprocessing time results in more divertable material.

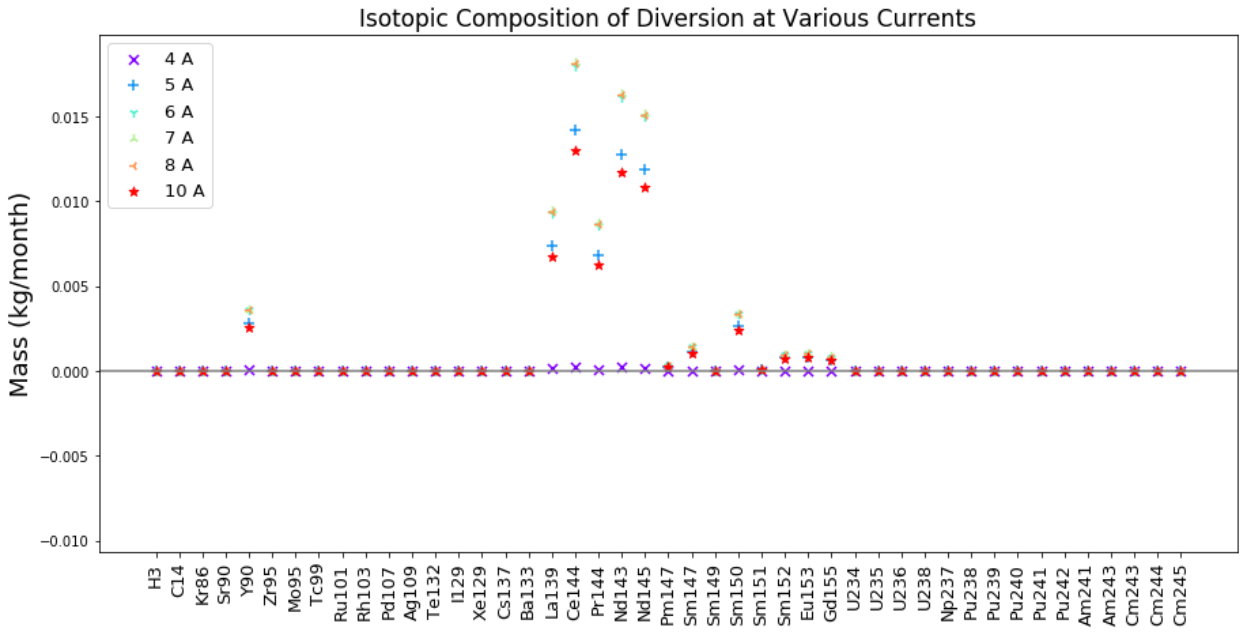

Figure 4.8: Isotopic composition of the diverted material stream at various electrowinner currents.

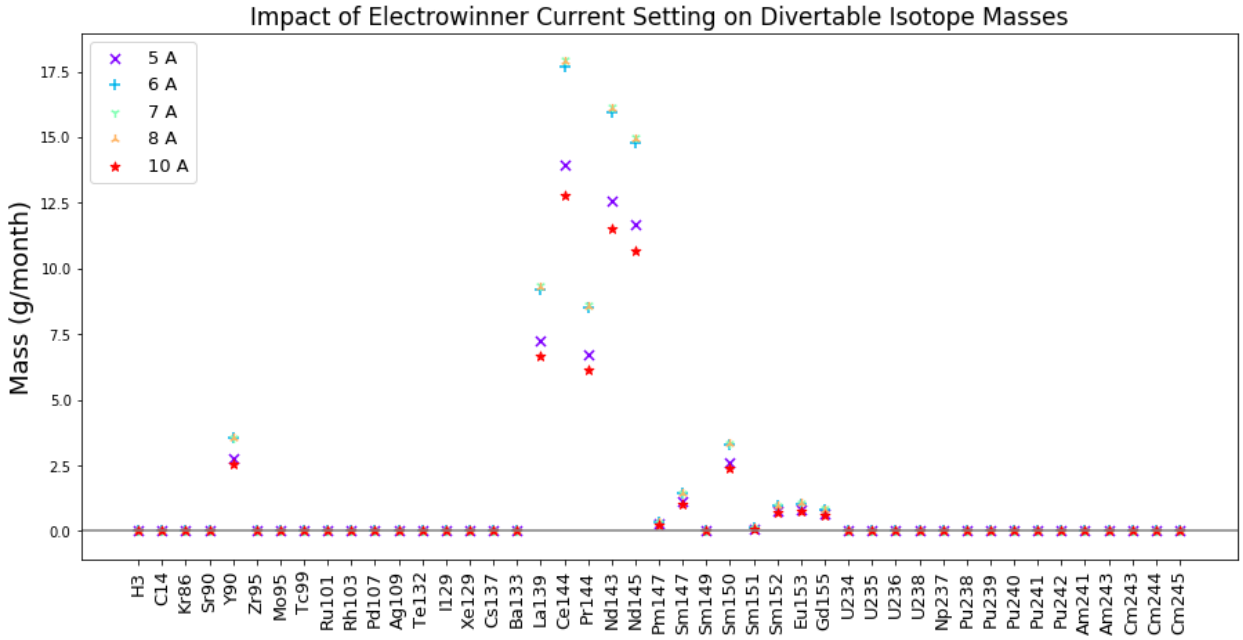

Figure 4.9: Isotopic composition of the diverted material stream at various electrowinner currents.

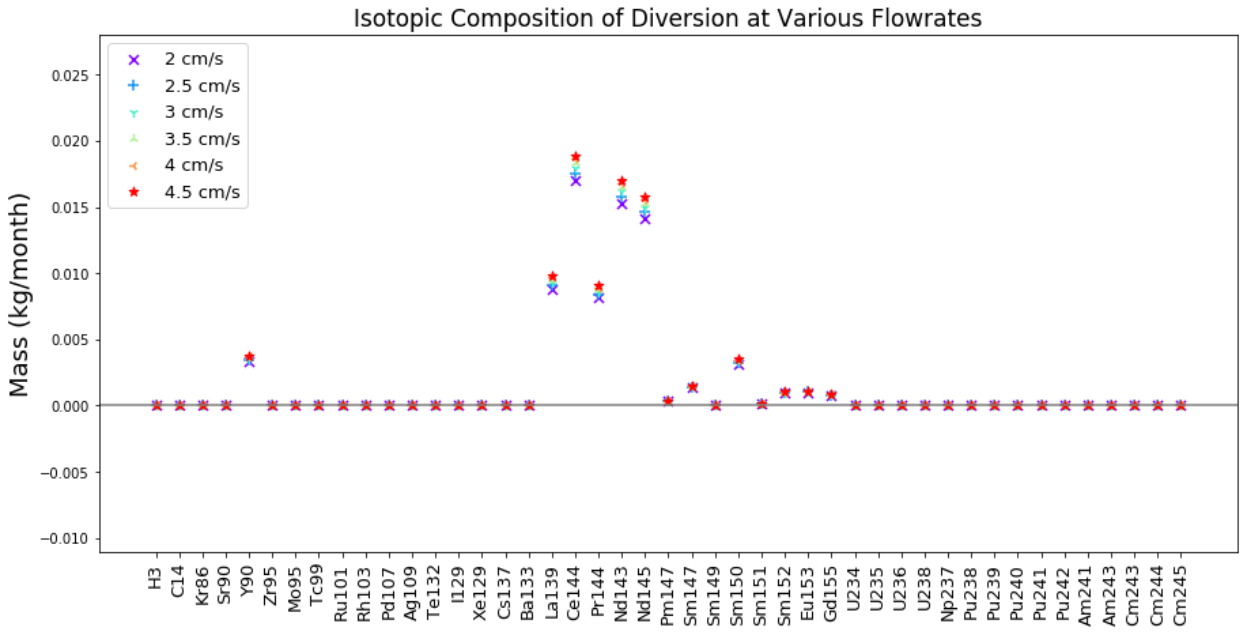

Figure 4.10: Isotopic composition of the diverted material stream at various electrowinner flowrates.

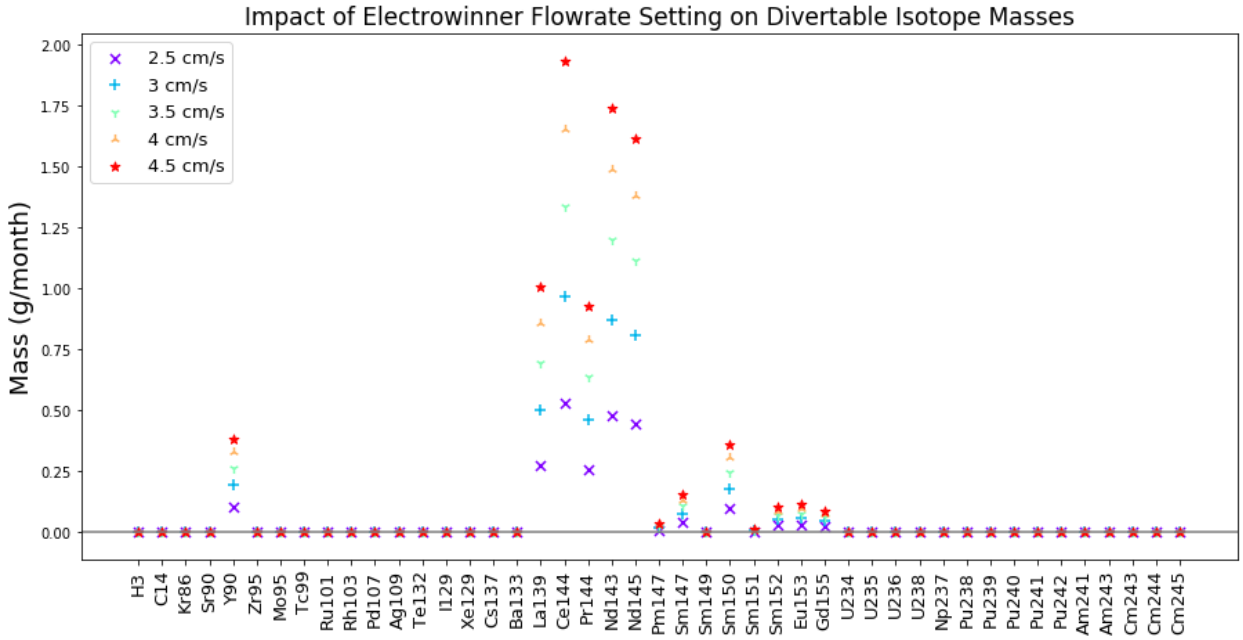

Figure 4.11: Isotopic composition of the diverted material stream at various electrowinner flowrates.

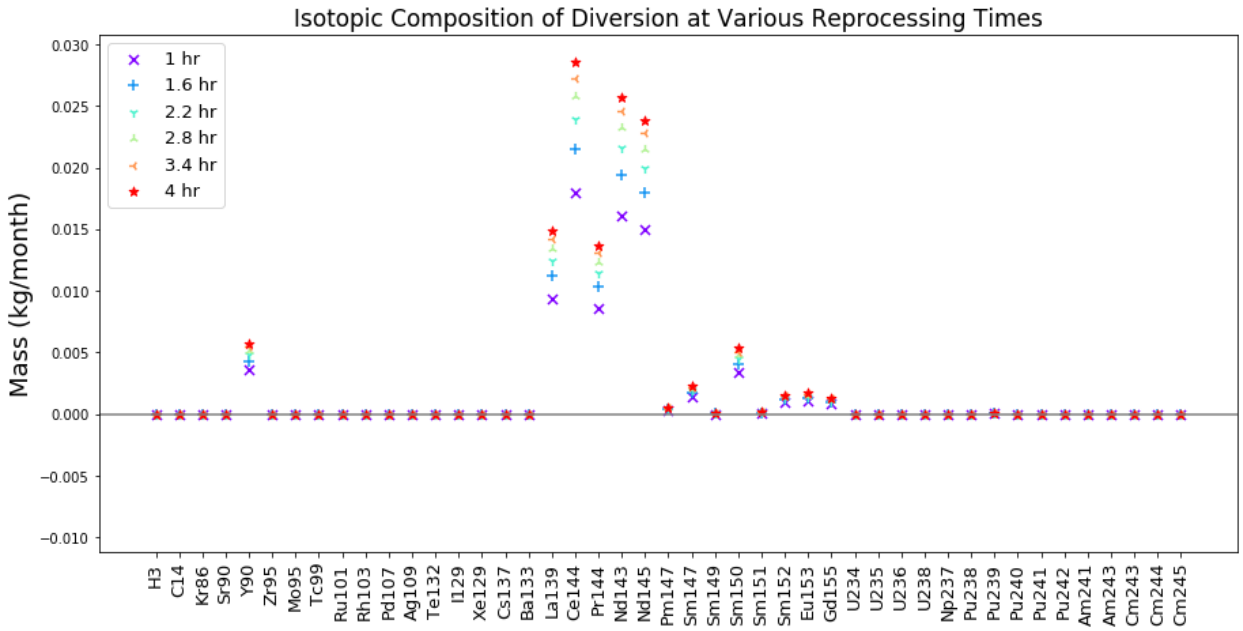

Figure 4.12: Isotopic composition of the diverted material stream at various electrowinner reprocessing durations.

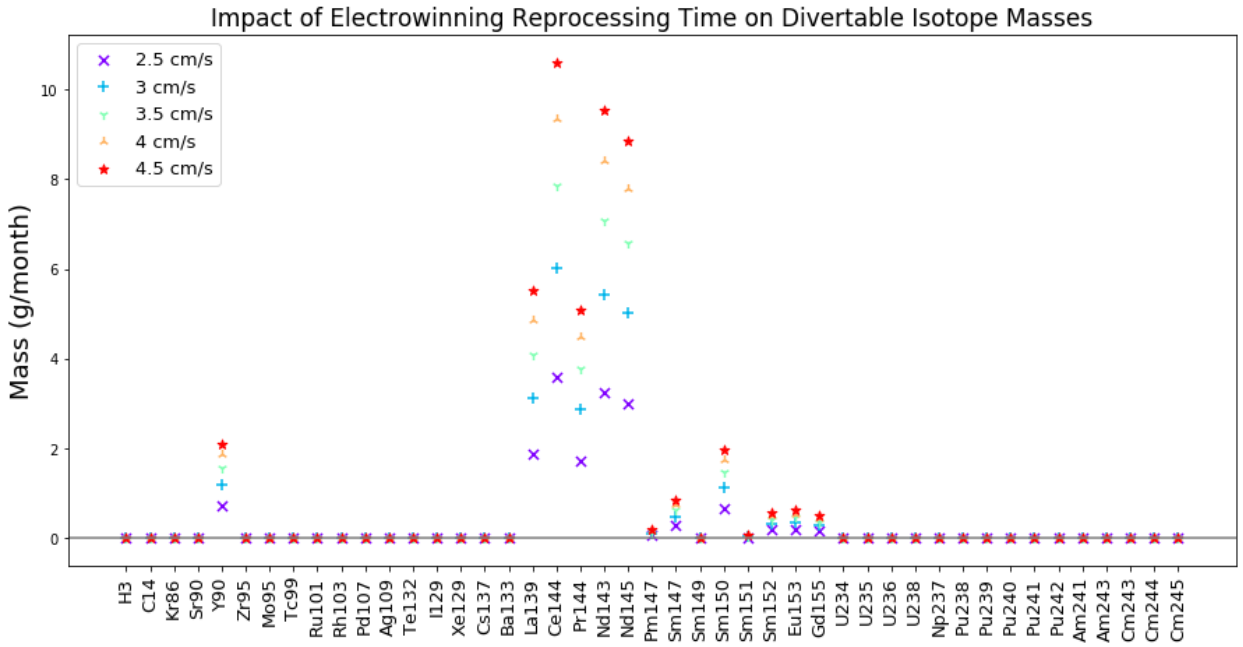

Figure 4.13: Isotopic composition of the diverted material stream at various electrowinner reprocessing durations.

4.4 Parameter Comparison

The material increase due to the previous six operational settings was normalized against their respective baseline to determine the most impactful process parameters. Table 4.2 summarizes these values.

Sample	ER Temp	ER Pressure	ER Stir Speed	EW Current	EW Flow rate	EW Time
1	0.036	8.589	30.284	5.684	3.136	20.030
2	0.715	13.336	33.542	7.216	5.699	33.602
3	0.975	15.393	35.447	7.308	7.866	43.879
4	1.672	15.912	36.799	7.281	9.743	52.154
5	3.328	16.047	37.848	5.202	11.398	59.080

Table 4.2: Comparison of operational settings' impact on divertable material (shown in % difference compared to baseline values). Where ER and EW represent electrorefiner and electrowinner respectively.

Sensitivity analysis for each setting is split into corresponding samples to reflect increasing efficiency. As we observed earlier, temperature and current, although primary settings, do not result in significant increase in separated material. Temperature alterations result in diminishing returns, as a drastic increase of heat is required for noticeably improved efficiency. Notably, the most impactful electrorefiner setting is the central stirrer's speed. The stirrer has such a significant impact due to increasing the rate of separation, and improving overall efficiency. Comparing the stirrer and pressure separation efficiency illuminates the stirrer's significance. Reducing pressure to 100 mTorr results in a 16% increase in material while a stirrer at 20 rpm nearly doubles that at 30.284% increase. Separation efficiency due to changes in current plateaus because the process is limited by reaction rate. Increasing electrowinner current does not affect opportunity to react as flowrate and time can be seen to do. A trend noticed in these settings is those which allow more interaction between the salt and waste see a more significant increase in product.

While the rest also result in improved efficiency, they require a larger change in operation to meet the same increased separation.

Chapter 5

Conclusion

This thesis was motivated by a lack of medium fidelity pyroprocessing plant models in current fuel cycle simulators [6]. Combined with the need for safeguards-by-design in next generation nuclear fuel cycle facilities, a pyroprocessing facility model with diversion capabilities fills these technological gaps in safeguarding future fuel cycles. This work designed, implemented, and demonstrated the Pyre software module. Pyre brings more detailed separations processes to nuclear fuel cycle simulators informed by more limited and specific electrochemical models such as SSPM and AMPYRE [5, 25]. The Pyre module resides within the `cyclus/recycle` repository, responsible for holding a library extension of reprocessing archetypes.

Cyclus provides a modular interface to expand and test the capabilities of reprocessing and material diversion. Pyre leverages this modular C++ framework and performed well in a full US fuel cycle transition from LWRs to SFRs using only Pyre facilities to facilitate this transition. Observing the transition scenario's uranium utilization, TRU production, and successful fueling and operation of SFRs to meet power demands verifies Pyre's role in the simulation.

We also used this transition scenario to test the sensitivity of key operational settings in a diversion scenario. Using Dakota to vary key settings of the electrorefiner and electrowinner, we determined the impact of each setting on product efficiency. Processes that improved interfacing between the eutectic salt and metallic waste, such as electrorefiner stirring, electrowinner flowrate, and electrowinner reprocessing time, were found to most significantly impact separation efficiency.

5.1 Future Work

This work has laid the groundwork for further research into diversion detection algorithms and sub-facility modeling. The current CUSUM implementation can only focus on a single data stream per diversion scenario. A more complex, nuanced method capable of accounting for multiple parameters simultaneously would better inform users of potential diversion. Another aspect to be improved is the fidelity of the pyroprocessing system itself. This can be approached in a couple ways, reducing the timestep or comparing with experimental data.

Smaller timesteps will provide frequent data allowing more complex diversion scenarios and more detailed change detection algorithms. Rather than diverting for an entire month at a time, these scenarios could operate on a per batch basis. Likewise, further experimental data would help synergy between multiple settings at once. In addition to improving model fidelity, this would serve to validate separation performance and facility capabilities.

References

[1] "Serving Nuclear Non-Proliferation," 2017. [Online]. Available: https://www.iaea.org/sites/default/files/17/12/sg-serving-nuclear-non-proliferation.pdf

[2] K. D. Huff, M. J. Gidden, R. W. Carlsen, R. R. Flanagan, M. B. McGarry, A. C. Opotowsky, E. A. Schneider, A. M. Scopatz, and P. P. H. Wilson, "Fundamental concepts in the Cyclus nuclear fuel cycle simulation framework," *Advances in Engineering Software*, vol. 94, pp. 46–59, Apr. 2016. [Online]. Available: http://www.sciencedirect.com/science/article/pii/S0965997816300229

[3] R. Wigeland, T. Taiwo, H. Ludewig, M. Todosow, W. Halsey, J. Gehin, R. Jubin, J. Buelt, S. Stockinger, K. Jenni, and B. Oakley, "Nuclear Fuel Cycle Evaluation and Screening - Final Report," *US Department of Energy*, p. 51, 2014. [Online]. Available: https://fuelcycleevaluation.inl.gov/Shared%20Documents/ES%20Main%20Report.pdf

[4] I. A. E. Agency, Ed., *Implications of partitioning and transmutation in radioactive waste management*, ser. Technical report series. Vienna: International Atomic Energy Agency, 2004, no. no. 435, oCLC: ocm59136942.

[5] L. E. Maggos, C. Pereira, J. A. F. Caputo, and J. M. Copple, "Update on Electrochemical Mass Balance Modeling for Safeguards," p. 13, 2015.

[6] R. A. Borrelli, J. Ahn, and Y. Hwang, "Approaches to a practical systems assessment for safeguardability of advanced nuclear fuel cycles," *Nuclear Technology*, vol. 197, pp. 248–264, Mar. 2017.

[7] Michael F. Simpson, "Developments of Spent Nuclear Fuel Pyroprocessing Technology at Idaho National Laboratory," Tech. Rep. INL/EXT-12-25124, 1044209, Mar. 2012. [Online]. Available: http://www.osti.gov/servlets/purl/1044209/

[8] H. Lee, J. H. Lee, S. B. Park, Y. S. Lee, E. H. Kim, and S. W. Park, "Advanced Electrorefining Process at KAERI," *ATALANTE*, May 2008. [Online]. Available: http://www.iaea.org/inis/collection/NCLCollectionStore/_Public/40/032/40032685.pdf

[9] A. A. Frigo, D. R. Wahlquist, and J. L. Willit, "A conceptual advanced pyroprocess recycle facility." Proc., American Nuclear Society : La Grange, IL, pp. 981-985, Tech. Rep. ANL/CMT/CP-111325, Jan. 2003. [Online]. Available: https://www.osti.gov/biblio/981298

[10] M. McGarry, "Mbmore," Oct. 2017.

[11] K. A. Mummah, "Material Diversion Analysis Within a Fuel Cycle Simulator," Champaign, IL, June 2019.

[12] S. E. Skutnik, N. C. Sly, and J. L. Littell, "CyBORG: An ORIGEN-Based Reactor Analysis Capability for Cyclus," in *Transactions of the American Nuclear Society*, ser. Fuel Cycle and Waste Management: General—II, vol. 115. Las Vegas, Nevada, United States: American Nuclear Society, Nov. 2016, pp. 299–301.

[13] E. Schneider and A. Scopatz, "An Integrated Fuel Depletion Calculator for Fuel Cycle Options Analysis," Tech. Rep. 12-4065, 1258475, Apr. 2016. [Online]. Available: http://www.osti.gov/servlets/purl/1258475/

[14] M. Hayyan, F. S. Mjalli, M. A. Hashim, I. M. AlNashef, and T. X. Mei, "Investigating the electrochemical windows of ionic liquids," vol. 19, no. 1, pp. 106–112. [Online]. Available: http://www.sciencedirect.com/science/article/pii/S1226086X12002353

[15] A. C. de Dios, "Introduction to electrochemistry," *GeorgeTown University*.

[16] Organisation for Economic Co-operation and Development, "Spent Nuclear Fuel Reprocessing Flowsheet," *Nuclear Energy Agency*, June 2012. [Online]. Available: https://www.oecd-nea.org/science/docs/2012/nsc-wpfc-doc2012-15.pdf

[17] R. Jubin, "Spent Fuel Reprocessing," Oak Ridge National Lab. (ORNL), Oak Ridge, TN (United States), Tech. Rep., 2009. [Online]. Available: http://www.cresp.org/NuclearChemCourse/monographs/07_Jubin_Introduction%20to%20Nuclear%20Fuel%20Cycle%20Separations%20-%20Final%20rev%202_3_2_09.pdf

[18] H. Ohta, T. Inoue, Y. Sakamura, and K. Kinoshita, "Pyroprocessing of Light Water Reactor Spent Fuels Based on an Electrochemical Reduction Technology," *Nuclear Technology*, vol. 150, no. 2, pp. 153–161, May 2005. [Online]. Available: https://doi.org/10.13182/NT05-A3613

[19] J.-M. Hur, C.-S. Seo, S.-S. Hong, D.-S. Kang, and S.-W. Park, "Electrochemical Reduction of Uranium Oxides in Li2o-LiCl Molten-salt," p. 7.

[20] Y. Sakamura, "Separation of Actinides from Rare Earth Elements by Electrorefining in LiCl-KCl Eutectic Salt," *J. Nucl. Sci. Technol.*, vol. 35, no. 1, pp. 49–59, Jan. 1998.

[21] S. Phongikaroon, "Introduction to Pyroprocessing Technology for Used Nuclear Fuel."

[22] H. Lee, J.-M. Hur, J.-G. Kim, D.-H. Ahn, Y.-Z. Cho, and S.-W. Paek, "Korean Pyrochemical Process R&D activities," *Energy Procedia*, vol. 7, pp. 391–395, 2011. [Online]. Available: http://linkinghub.elsevier.com/retrieve/pii/S1876610211015608

[23] R. W. Carlsen, M. Gidden, K. D. Huff, A. C. Opotowsky, O. Rakhimov, A. M. Scopatz, and P. Wilson, "Cycamore v1.0.0," June 2014.

[24] M. J. Gidden, "An agent-based modeling framework and application for the generic nuclear fuel cycle."

[25] B. B. Cipiti, F. A. Duran, B. R. Key, Y. Liu, I. Lozano, and R. Ward, "Modeling and design of integrated safeguards and security for an electrochemical reprocessing facility." Sandia National Laboratories, Tech. Rep. SAND2012-9303, Oct. 2012. [Online]. Available: https://www.osti.gov/biblio/1055891-modeling-design-integrated-safeguards-security-electrochemical-reprocessing-facility

[26] Organisation for Economic Co-operation and Development, "Spent Nuclear Fuel Reprocessing Flowsheet," *Nuclear Energy Agency*, June 2012. [Online]. Available: https://www.oecd-nea.org/science/docs/2012/nsc-wpfc-doc2012-15.pdf

[27] S. X. Li, T. A. Johnson, B. R. Westphal, K. M. Goff, and R. W. Benedict, "Electrorefining Experience for Pyrochemical Processing of Spent EBR-II Driver Fuel," no. 487, p. 7, 2005.

[28] E. Hou, Y. Yilmaz, and A. O. Hero, "Diversion detection in partially observed nuclear fuel cycle networks," 2016.

[29] Y. Yilmaz, E. Hou, and A. O. Hero, "Online diversion detection in nuclear fuel cycles via multimodal observations," 2016.

[30] E.-Y. Choi and S. M. Jeong, "Electrochemical processing of spent nuclear fuels: An overview of oxide reduction in pyroprocessing technology," *Progress in Natural Science: Materials International*, vol. 25, no. 6, pp. 572–582, Dec. 2015. [Online]. Available: http://linkinghub.elsevier.com/retrieve/pii/S1002007115001197

[31] H. Lee, H. Suk Im, and G. Il Park, "Modeling of oxide reduction in repeated-batch pyroprocessing," *Annals of Nuclear Energy*, vol. 88, pp. 1–11, Feb. 2016. [Online]. Available: http://linkinghub.elsevier.com/retrieve/pii/S0306454915005174

[32] H. Lee, J. H. Lee, S. B. Park, Y. S. Lee, E. H. Kim, and S. W. Park, "Advanced Electrorefining Process at KAERI," *ATALANTE 2008*, May 2008. [Online]. Available: http://www.iaea.org/inis/collection/NCLCollectionStore/_Public/40/032/40032685.pdf

[33] T. Koyama, Y. Sakamura, M. Iizuka, T. Kato, T. Murakami, and J.-P. Glatz, "Development of Pyro-processing Fuel Cycle Technology for Closing Actinide Cycle," *Procedia Chemistry*, vol. 7, pp. 772–778, 2012. [Online]. Available: http://linkinghub.elsevier.com/retrieve/pii/S187661961200191X

[34] T.-J. Kim, G.-Y. Kim, D. Yoon, D.-H. Ahn, and S. Paek, "Development of an anode structure consisting of graphite tubes and a SiC shroud for the electrowinning process in molten salt," *Journal of Radioanalytical and Nuclear Chemistry*, vol. 295, no. 3, pp. 1855–1859, Mar. 2013. [Online]. Available: http://link.springer.com/10.1007/s10967-012-2103-5

[35] L. Chapman and C. Holcombe, "Revision of the uranium-iron phase diagram," *Journal of Nuclear Materials*, vol. 126, no. 3, pp. 323–326, Nov. 1984. [Online]. Available: http://linkinghub.elsevier.com/retrieve/pii/0022311584900461

[36] R. K. Ahluwalia, T. Q. Hua, and D. Vaden, "Uranium Transport in a High-Throughput Electrorefiner for EBR-II Blanket Fuel," *Nuclear Technology*, vol. 145, no. 1, pp. 67–81, Jan. 2004. [Online]. Available: https://www.tandfonline.com/doi/full/10.13182/NT04-A3461

[37] T.-H. Lee, Y.-S. Kim, T.-J. Kwon, H.-S. Shin, and H.-D. Kim, "Determination of the Plutonium Mass and Curium Ratio of Spent Fuel Assemblies for Input Nuclear Material Accountancy of Pyroprocessing, and Analysis of Their Errors," *Nuclear Technology*, vol. 179, no. 2, pp. 196–204, Aug. 2012. [Online]. Available: https://doi.org/10.13182/NT11-77

[38] "Non-Destructive Assay: Instruments and Techniques for Agency Safeguards," *IAEA Bulletin*, vol. 19, no. 5, pp. 34–37. [Online]. Available: https://www.iaea.org/sites/default/files/publications/magazines/bulletin/bull19-5/19503403437.pdf

[39] J. J. Duderstadt and L. J. Hamilton, *Nuclear Reactor Analysis*, 1st ed. New York: Wiley, Jan. 1976.

[40] M. Basseville and I. V. Nikiforov, *Detection of Abrupt Changes: Theory and Application*, ser. Prentice Hall information and system sciences series. Prentice Hall, Apr. 1993. [Online]. Available: ftp://ftp.irisa.fr/local/as/mb/k11.pdf

[41] M. Root and J. Miller, "SEE LANL - Nuclear Safeguards Training," LANL, Jan. 2019.